AZTEC CASTLES AND THE dP3 QUIVER

MEGAN LEONI, SETH NEEL, AND PAXTON TURNER

ABSTRACT. Bipartite, periodic, planar graphs known as *brane tilings* can be associated to a large class of quivers. This paper will explore new algebraic properties of the well-studied del Pezzo 3 quiver and geometric properties of its corresponding brane tiling. In particular, a factorization formula for the cluster variables arising from a large class of mutation sequences (called $\tau-$mutation sequences) is proven; this factorization also gives a recursion on the cluster variables produced by such sequences. We can realize these sequences as walks in a triangular lattice using a correspondence between the generators of the affine symmetric group $\tilde{A}_2$ and the mutations which generate $\tau-$mutation sequences. Using this bijection, we obtain explicit formulae for the cluster that corresponds to a specific alcove in the lattice. With this lattice visualization in mind, we then express each cluster variable produced in a τ-mutation sequence as the sum of weighted perfect matchings of a new family of subgraphs of the dP3 brane tiling, which we call *Aztec castles*. Our main result generalizes previous work on a certain mutation sequence on the dP3 quiver in [Zha12], and forms part of the emerging story in combinatorics and theoretical high energy physics relating cluster variables to subgraphs of the associated brane tiling.

Date: September 5, 2013.
2000 *Mathematics Subject Classification.* 13F60, 05C30, 05C70.
Key words and phrases. cluster algebras, combinatorics, graph theory, brane tilings.
The authors were supported by NSF Grants DMS-#1067183 and DMS-#1148634.

Contents

1. Introduction

First introduced and pioneered by Fomin and Zelevinsky in [FZ] to study total positivity and dual canonical bases in semisimple Lie groups, cluster algebras have found a wealth of applications in many branches of mathematics including combinatorics, tropical geometry [SW], Teichmuller theory [FG], and representation theory [Kel08]. Cluster algebras are classes of commutative rings whose generators, known as cluster variables, are partitioned into subsets known as clusters. An iterative process called seed mutation provides a link between clusters and can be used to recover the complete set of generators given an initial seed [Zel07].

Meanwhile, theoretical physics has made intriguing advancements into the study of doubly-periodic, bipartite, planar graphs, known as brane tilings. These appear physically in string theory through the intersections of NS5 and D5-branes which are dual to a configuration of D3-branes probing the singularity of a toric Calabi-Yau threefold [FHK$^+$]. Brane tilings are inherently connected to the geometry of the threefold as well as the $(3+1)$ dimensional supersymmetric gauge field theory that lives on the worldvolume of the D3-brane, which can be represented by a directed graph known as a quiver. There is significant interest in giving combinatorial interpretations for cluster variables arising from such quivers, see for example [MS],[LS],[Mus]. Recent research has related a single mutation sequence on the quiver associated to the third del Pezzo surface to a class of subgraphs of its brane tiling known as Aztec dragons [Zha12],[CY10]. This paper generalizes the work in [Zha12] by relating an infinite class of mutation sequences to a new, broader class of subgraphs of the brane tiling which we call **Aztec castles**.

1.1. Quivers and Brane Tilings.

A **quiver** Q is a directed finite graph with a set of vertices V and a set of edges E connecting them whose direction is denoted by an arrow. For our purposes Q may have multiple edges connecting two vertices but may not contain any loops or $2-$cycles. We can relate a cluster algebra with initial seed $\{x_1, x_2, \ldots, x_n\}$ to Q by associating a cluster variable x_i to every vertex labeled i in Q where $|V| = n$. The cluster is the union of the cluster variables at each vertex.

Definition 1. ***Quiver Mutation:*** *Mutating at a vertex i in Q is denoted by μ_i and corresponds to the following actions on the quiver:*

- *For every 2-path through i (e.g. $j \to i \to k$), add an edge from j to k.*
- *Reverse the directions of the arrows incident to i*
- *Delete any 2-cycles created from the previous two steps.*

When we mutate at a vertex i, the cluster variable at this vertex is updated and all other cluster variables remain unchanged [JMZ13]. The action of μ_i on the cluster leads to the following binomial exchange relation:

$$x_i' x_i = \prod_{i \to j \text{ in } Q} x_j^{a_{i\to j}} + \prod_{j \to i \text{ in } Q} x_j^{b_{j\to i}}$$

where x_i' is the new cluster variable at vertex i, $a_{i\to j}$ denotes the number of edges from i to j, and $b_{j\to i}$ denotes the number of edges from j to i.

Quivers describing gauge theories on the worldvolume of D3-branes probing toric Calabi-Yau singularities are also intimately connected to another planar graph known as a **brane tiling** (or dimer model). Unfolding the quiver onto the plane while maintaining the same edge connections leads to an infinite planar graph. The dual of this graph is the brane tiling; a bipartite, doubly-periodic, planar graph.

Our main object of study is the quiver Q associated to the third del Pezzo surface (**dP3**), illustrated in Figure 1 with its associated brane tiling [FHK$^+$], [HS]. Note that later on, we will refer to a hexagon in the brane tiling consisting of the quadrilaterals (given in clockwise order) $5-3-1-4-2-0$ as a **6-cycle**.

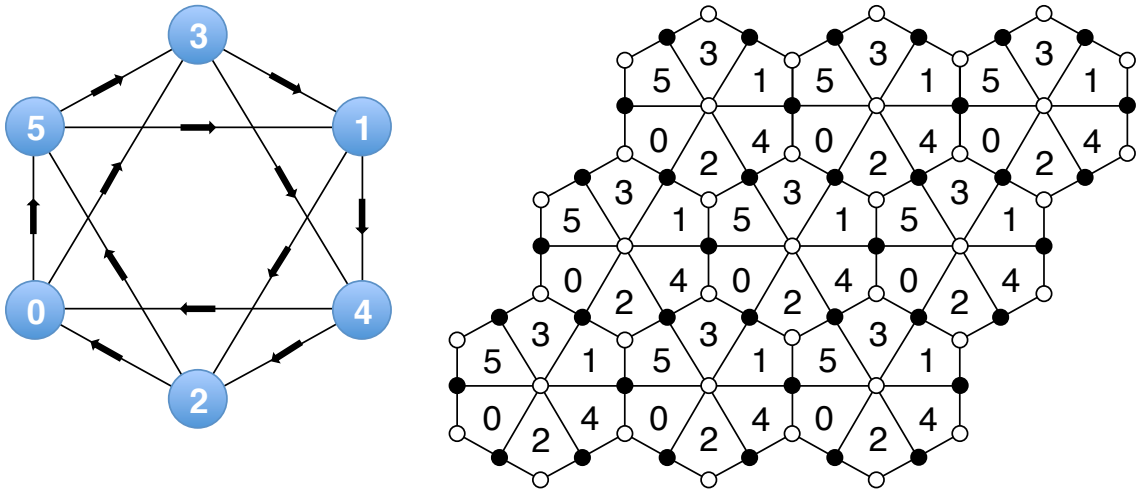

FIGURE 1. The dP3 quiver Q [**Left**] and its associated brane tiling [**Right**], a doubly periodic, bipartite graph that is the planar dual to the unfolded quiver.

We can describe in more detail the unfolding process for this specific quiver in the manner of [JMZ13] (a description for generic quivers can be found where the procedure was first introduced in [FHK$^+$]). Denote by E_{ij} the boundary edge from vertex i to j in our labeling of Q. The dP3 brane tiling is associated to the following formal linear combination of closed cycles of the quiver, known as a *superpotential* (W) in a supersymmetric gauge theory where each edge in the unit cell of the brane tiling appears exactly twice, once for clockwise (positive) orientation and once for counter-clockwise (negative) orientation.

$$\begin{aligned} W = {} & E_{31}E_{14}E_{42}E_{20}E_{05}E_{53} + E_{34}E_{40}E_{03} + E_{12}E_{25}E_{51} \\ & - E_{14}E_{40}E_{05}E_{51} - E_{34}E_{42}E_{25}E_{53} - E_{31}E_{12}E_{20}E_{03} \end{aligned}$$

We can now *unfold* Q into a planar digraph $\tilde{Q}$ composed of the given cycles such that the local configuration about vertex i is the same in $\tilde{Q}$ and Q , exhibited in Figure 2. The brane tiling illustrated in Figure 1 is exactly the dual graph to $\tilde{Q}$,

where bipartiteness is created by placing white vertices in positively oriented cycles and black vertices in negatively oriented cycles.

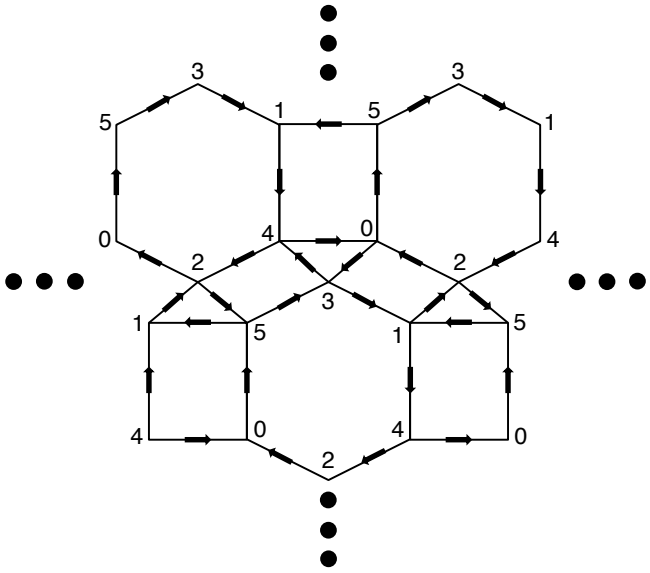

FIGURE 2. A section of the unfolded dP3 quiver $\tilde{Q}$.

1.2. **τ-mutation Sequences.** Here we define a class of mutation sequences on Q which we refer to as τ -mutation sequences. The action of each τ mutates at antipodal vertices and has a symmetrical action on the quiver. This symmetry underlies the proofs of all of our main results.

Definition 2. *Define the following pairs of mutations on Q.*

$$\tau_1 = \mu_0 \circ \mu_1$$
$$\tau_2 = \mu_2 \circ \mu_3$$
$$\tau_3 = \mu_4 \circ \mu_5$$

One can then check that for all i, j such that $1 \leq i \neq j \leq 3$

$$(\tau_i)^2 = \mathrm{id}$$
$$(\tau_i \tau_j)^3 = \mathrm{id}.$$

We observe that the action of τ_i on the quiver exchanges the labels on vertices $2i-2$ and $2i-1$. Furthermore, since antipodal vertices share no common edges, μ_{2i-1} and μ_{2i-2} commute for $i \in \{1, 2, 3\}$.

A **τ-mutation sequence** is a mutation sequence of the form $\tau_{a_1}\tau_{a_2}\tau_{a_3}\ldots$. From now on we will abbreviate such a mutation sequence by its subscripts $a_1a_2a_3\ldots$. The cluster variables produced after $\tau_{a_n} = \mu_i \circ \mu_{i+1}$ in such a sequence are denoted by y_n and y'_n where y_n is the variable produced by μ_i and y'_n is the variable produced by the latter mutation μ_{i+1} in τ_{a_n}. By the symmetry of Q, y_n and y'_n are related by the action of the permutation $\sigma = (01)(23)(45)$ which flips antipodes, i.e. $\sigma y_n = y'_n$. It is also worth noting that σ acts on the brane tiling as a 180° rotation.

1.3. **Preliminary Definitions and Aztec Dragons.** We will adopt the weighting scheme on the brane tiling utilized in [Zha12] by Zhang, in [Spe] by Speyer, and in [GK12] by Goncharov–Kenyon which we will now describe. Associate the **weight** $\frac{1}{x_i x_j}$ to each edge bordering faces labeled i and j in the brane tiling. Let $M(G)$ denote the set of perfect matchings in a subgraph G of the brane tiling respectively. We define the weight of a perfect matching in the usual manner as the product of the weights of the edges included in the matching under the weighting scheme. Then we define the weight of G as

$$w(G) = \sum_{M \in M(G)} w(M).$$

Similarly we can define the **covering monomial**, $m(G)$, of an induced subgraph G of the brane tiling as the monomial $x_0^{a_0} x_1^{a_1} x_2^{a_2} x_3^{a_3} x_4^{a_4} x_5^{a_5}$, where a_j is the number of faces labeled j enclosed in or bordering G[1]. Figure 3 illustrates an example of the quadrilaterals included in the covering monomial of a small subgraph, outlined in red.

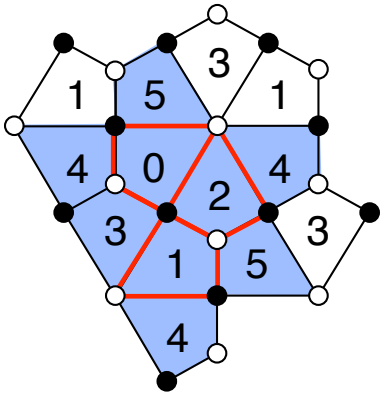

FIGURE 3. The covering monomial of the subgraph outlined in red includes the blue quadrilaterals and is given by $x_0 x_1 x_2 x_3 x_4^3 x_5^2$.

Finally, to make notation more concise in later proofs, it will be useful to define the product of the covering monomial and weight of a subgraph G as

$$c(G) = w(G)m(G).$$

Zhang studied the mutation sequence $123123\ldots$ in [Zha12] and found that the cluster variable obtained after each mutation in the sequence can be expressed as the weighted perfect matchings of a family of subgraphs of the dP3 brane tiling. In fact these graphs turned out to be the family of **Aztec dragons** $\{D_{n/2}\}_{n \in \mathbb{N}}$ introduced and enumerated in [CY10]. The first few Aztec dragons are exhibited in Figure 4. Specifically in the notation described above, Zhang proved that $y_n = c(D_{n/2})$

[1]The covering monomial has a more general definition suitable for other contexts. See [Jeo11] and [JMZ].

(respectively, $y'_n = c(\sigma D_{n/2})$). Zhang's findings have provided the starting point for our main contribution: relating the weighted perfect matchings of subgraphs of the dP3 brane tiling to cluster variables for all possible τ-mutation sequences.

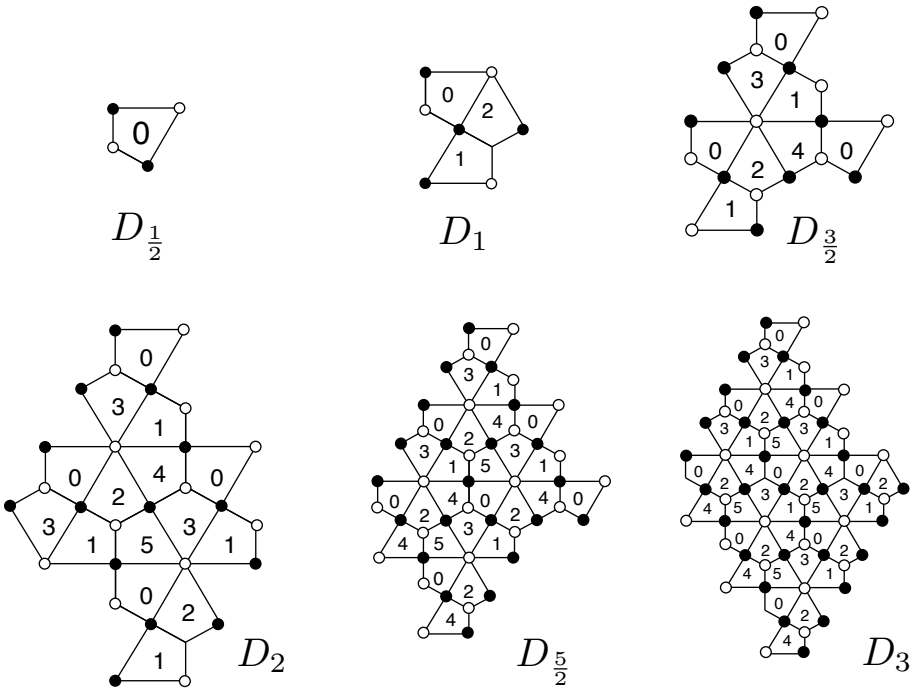

FIGURE 4. Examples of the Aztec dragons $D_{n/2}$.

1.4. **Main Results.** We are now equipped to state our main theorem, which relates cluster variables produced by τ-mutation sequences to a new family of subgraphs in the brane tiling. This family, which we call **Aztec castles**, will be defined later in Section 4.2 and presents a generalization of the Aztec dragons introduced in [CY10] and studied in [Zha12].

Theorem 1.1 (Main Theorem)**.** *For any $\tau-$mutation sequence on the dP3 quiver we can associate a subgraph G of the brane tiling to each cluster variable y_n (resp. y'_n) produced such that*

$$y_n = c(G)$$

and respectively, $y'_n = c(\sigma G)$.

Along the way we also obtain:

- A factorization formula for cluster variables produced in τ-mutation sequences on the dP3 quiver (Section 2.1). This combined with the main result implies that all Aztec castles have 2^k perfect matchings.
- A recursion which enables efficient calculation of cluster-variables arising in any τ-mutation sequence. (Section 2.2)

- Existence of explicit formulae for the cluster variables produced by any τ-mutation sequence. (Section 3)

Sections 4 and 5 describe the Aztec castles appearing in the integer and half-integer cone, respectively. The proof of our main theorem follows from the results in these sections (Theorems 4.4 and 5.1) and a brief symmetry argument presented in Section 3. We conclude the introduction with the following construction for visualizing τ-mutation sequences.

1.5. **Coxeter Lattice and Relations.** We will now introduce a useful construction, a triangular lattice associated to the Coxeter group $\tilde{A}_2$ which we shall call the *Coxeter lattice* [Rou]. This lattice allows for a clear visualization of τ-mutation sequences. We will identify two important regions on the Coxeter lattice: the **integer** and **half-integer cones**. Finally, we place coordinates on these regions in terms of what we call **canonical paths**. These constructions will be pivotal in later sections.

The relations observed amongst the τ_j's (introduced directly after Definition 2) coincide with the relations amongst the generators of the affine symmetric group $\tilde{A}_2$. In Section 3 we verify that indeed these are the only relations amongst the τ_j's; this result also follows as an easy corollary of our main theorem. Then we can view any mutation sequence (word in the τ_j's), as a gallery of alcoves (faces in the triangular lattice) associated to $\tilde{A}_2$. Hence there is a bijection between clusters produced by τ-mutation sequences and alcoves in the lattice.

Each triangle in the lattice has edges labeled with a permutation of $\{1, 2, 3\}$. We fix the shaded (purple) triangle as the origin and label its edges as shown in Figure 5. Then we label the rest of the edges in the lattice according to the following rule: given a labeled triangle, we label any triangle that shares an edge with the labeled triangle by reflecting the labels over the shared edge. This gives a well-defined labeling on the entire lattice after choosing an initial labeling of the origin. Beginning at the origin (initial cluster), mutation by τ_i corresponds to moving to the adjacent alcove that shares the edge labeled i with the origin. Figure 5 exhibits the lattice, with marked mutation sequences drawn as paths that split the lattice into twelve disjoint regions.

The region labeled I (light blue), which we dub the **integer cone**, consists of:

(1) All alcoves intersected by the path $123123\ldots$ after an even number of steps, including the original alcove containing the initial cluster.
(2) All alcoves intersected by the path $12131213\ldots$ after its second step.
(3) All alcoves between those listed in the previous two bullets.

The region labeled XII (orange), which we dub the **half-integer cone**, is defined similarly to include:

(1) All alcoves intersected by the path $123123\ldots$ after an odd number of steps.
(2) All alcoves intersected by the path $12321232\ldots$ after its second step.
(3) All alcoves between those listed in the previous two bullets.

Now we put a coordinate system on the integer cone and half-integer cone. First fix the purple alcove in Figure 5 to be the initial cluster.

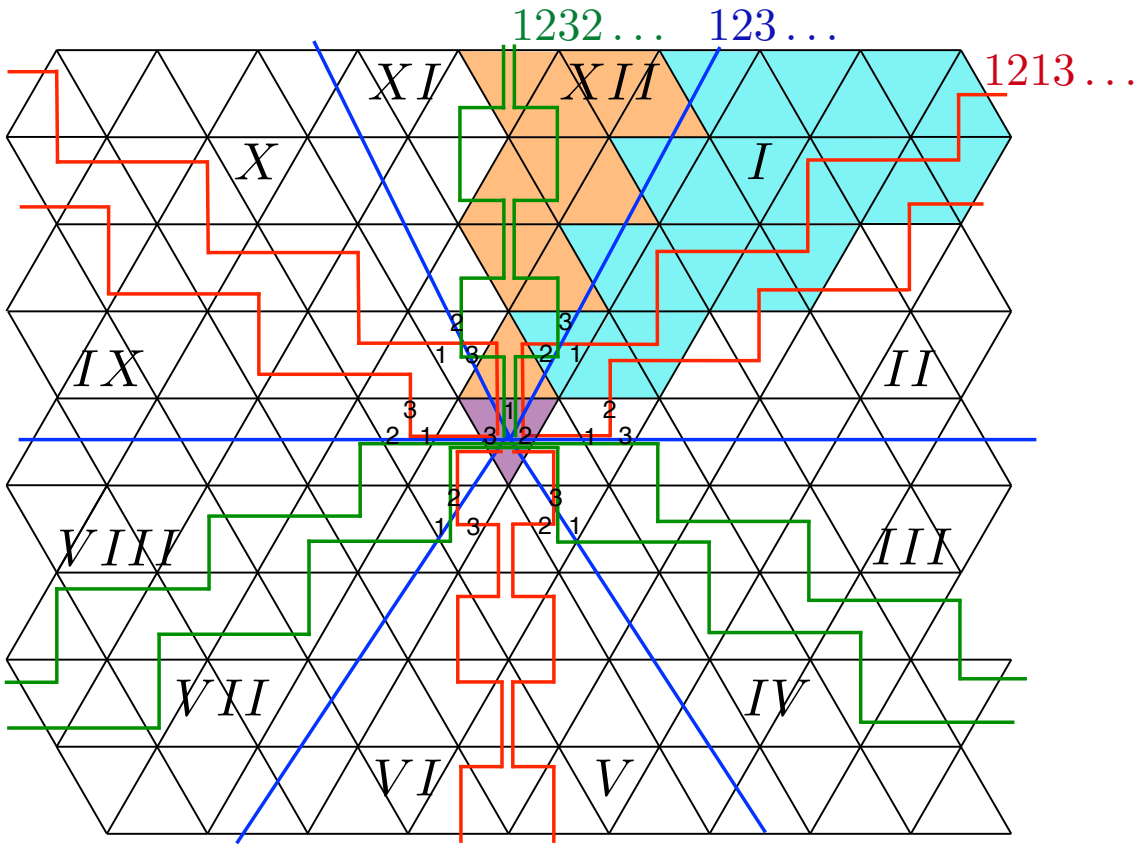

FIGURE 5. The lattice associated to the affine symmetric group $\tilde{A}_2$ which provides a visualization of τ-mutation sequences as walks. Blue paths represent 123123... sequences and permutations thereof, while red and green paths correspond to 12131213... and 12321232... type sequences respectively.

A **canonical path** in the integer cone consists of two components. The first includes crossing j horizontal lines after $2j$ steps on the blue path 123123.... We label the alcoves met by this first component as $(0, j)$. At some height j, a canonical path may turn horizontal. This turning point is indicated by a vertical line $|$. In this notation, the canonical paths in the integer cone have the following form based on the value of $j \mod 3$. Let $\beta = 123$.

(1) $\beta^{\frac{1}{3}(2j-1)}1|(321321\ldots)$ if $j \equiv 2 \mod 3$
(2) $\beta^{\frac{2}{3}j}|(213213\ldots)$ if $j \equiv 0 \mod 3$
(3) $\beta^{\frac{2}{3}(j-1)}12|(132132\ldots)$ if $j \equiv 1 \mod 3$

A path whose turning point is at height j can continue horizontally for at most $2j$ steps (after this, the path would leave the integer cone). Note that the last four horizontal steps possible intersect the path 1213..., the other boundary of the integer cone.

Now we can label the entire integer cone with coordinates. An alcove $\mathcal{A}$ in the integer cone has coordinates (i, j) if the canonical path to $\mathcal{A}$ crosses j horizontal lines before the turning point marked by $|$ and crosses i edges after the turning point. This is illustrated in Figure 6 with a canonical path to the alcove labeled $(3, 3)$.

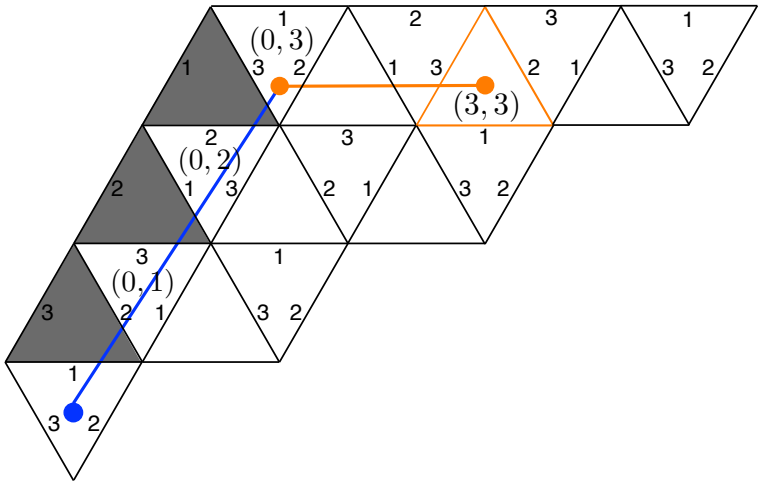

FIGURE 6. The canonical path to alcove labelled (i, j) which is in this example is $(3, 3)$. The blue path corresponds to the mutation sequence $\{\tau_1, \tau_2, \tau_3, \ldots\}$ and the orange horizontal path corresponds to $\{\tau_2, \tau_1, \tau_3 \ldots\}$ and leads to the desired alcove.

Now we describe canonical paths and coordinates on the half-integer cone. The first component of a canonical path begins at the previously marked initial cluster and consists of crossing $j + 1$ horizontal lines after $2j + 1$ steps on the $123123\ldots$ mutation sequence path. We label the alcoves met by this first component as $(0, j)$. These paths continue after the turning point, indicated by $|$ as before, for at most $2j$ steps. In terms of $j \mod 3$, canonical paths have the following form:

(1) $\beta^{\frac{1}{3}(2j+1)}|(213213\ldots)$ if $j \equiv 1 \mod 3$
(2) $\beta^{\frac{1}{3}(2j-1)}12|(132132\ldots)$ if $j \equiv 2 \mod 3$
(3) $\beta^{\frac{2}{3}j}1|(321321\ldots)$ if $j \equiv 0 \mod 3$

Note that, after the turning point, the final four steps possible in the path intersect the sequence $12321232\ldots$. We say that an alcove $\mathcal{A}$ in the half-integer cone has coordinates (i, j) if the canonical path to $\mathcal{A}$ crosses $j + 1$ horizontal lines before the turning point marked by $|$ and crosses i edges after the turning point. For example, the alcove traced by the path $12312|(132)$ has coordinates $(3, 2)$ as exhibited in Figure 7.

Coordinates and canonical paths in the remaining regions $II - XI$ are defined in an analogous way, using a permuted $123\ldots$ path as the vertical axis.

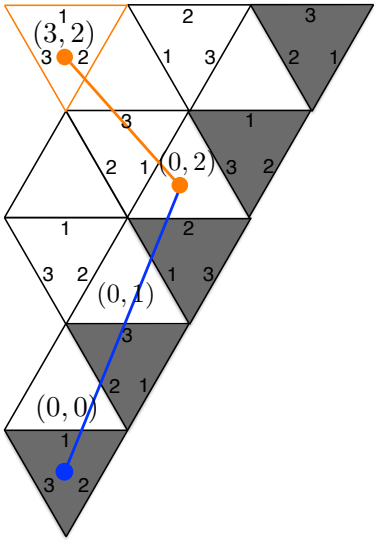

FIGURE 7. The canonical path to alcove labeled (i, j) in the half integer cone which in this example is $(3, 2)$.

2. The Factorization Phenomenon

We first prove a general factorization theorem for clusters arising from τ-mutation sequences. As a corollary to this factorization theorem we obtain a recursion on the cluster variables, an explicit formula for the clusters in the $123123\ldots$ sequence, an explicit formula for the $12131213\ldots$ sequence, and a generating function for the dragons studied in [Zha12] and [CY10].

2.1. **Factorization of cluster variables.** First we introduce some convenient notation. Suppose that we have a τ-mutation sequence $S = a_1a_2a_3a_4\ldots$. Denote by $\eta(n, i)$ the number of times we have mutated at vertex i in the first n terms ($2n$ total mutations) of S. Furthermore, let $C_n(Q)$ denote the ordered cluster obtained after applying n terms of S. Let $A = \frac{x_2x_4+x_3x_5}{x_0x_1}, B = \frac{x_1x_4+x_0x_5}{x_2x_3}, C = \frac{x_0x_2+x_1x_3}{x_4x_5}$. Finally, define the following six functions. For $i = 0, 2, 4$, we set

$$f_i(n) = \begin{cases} i & \text{if } \eta(n, i) = 0 \bmod 2 \\ i + 1 & \text{else} \end{cases}$$

and for $i = 1, 3, 5$, we set

$$f_i(n) = \begin{cases} i & \text{if } \eta(n, i) = 0 \bmod 2 \\ i - 1 & \text{else} \end{cases}$$

.

Theorem 2.1. *Fix $S = a_1a_2a_3a_4\ldots$ to be any $\tau-$mutation sequence on Q. The cluster $C_n(Q)$ has the following form:*

$$C_n(Q) = \{x_{f_0(n)}A^{a_1}B^{b_1}C^{c_1}, x_{f_1(n)}A^{a_1}B^{b_1}C^{c_1}, x_{f_2(n)}A^{a_2}B^{b_2}C^{c_2},$$
$$x_{f_3(n)}A^{a_2}B^{b_2}C^{c_2}, x_{f_4(n)}A^{a_3}B^{b_3}C^{c_3}, x_{f_5(n)}A^{a_3}B^{b_3}C^{c_3}\}.$$

Proof. Call the above form for the cluster variables a $\tau-$presentation, and the $x_{f_i(n)}$ term in each factorization the *leading term*. We induct on the cluster $C_n(Q)$. After applying any initial τ_i the cluster has the above form, so this is our base case. Assume that $C_n(Q)$ has a τ-presentation and mutate at vertex 0. Denote the cluster variable at vertex i in $C_n(Q)$ by X_i. It suffices to show that X_0', the variable produced at vertex 0 after applying τ_1, has $\tau-$presentation $x_{f_0(n+1)}A^{a_1'}B^{b_1'}C^{c_1'}$; the cases of mutating at other vertices are analogous.

Note that by the symmetry of the quiver, $\sigma(X_i) = X_{\sigma(i)}$. Each τ_i has action on the quiver that simply relabels the vertices by switching vertex $2i-1$ with vertex $2i-2$. Moreover, when we mutate by τ_i, $\eta(n, 2i-1)$ and $\eta(n, 2i-2)$ increase by 1, which by inductive assumption flips the leading terms of the cluster variables at vertices $2i-1$ and $2i-2$. Since each vertex i has leading term x_i in the initial cluster, for the purposes of the exchange at vertex 0, we can assume WLOG each cluster variable in $C_n(Q)$ has $f_i(n) = i$, and that the quiver has the original labeling. This is because the two vertices with arrows pointing to vertex 0 always have leading terms x_2 and x_4, the two vertices that vertex 0 points to have leading terms x_3 and x_5, and this property is invariant under a $\tau-$mutation. Now let

$$X_5 = x_5\left(\frac{x_2x_4+x_3x_5}{x_0x_1}\right)^{a_1}\left(\frac{x_1x_4+x_0x_5}{x_2x_3}\right)^{b_1}\left(\frac{x_0x_2+x_1x_3}{x_4x_5}\right)^{c_1},$$

then

$$X_4 = \sigma(X_5) = x_4\left(\frac{x_2x_4+x_3x_5}{x_0x_1}\right)^{a_1}\left(\frac{x_1x_4+x_0x_5}{x_2x_3}\right)^{b_1}\left(\frac{x_0x_2+x_1x_3}{x_4x_5}\right)^{c_1},$$

let

$$X_3 = x_3\left(\frac{x_2x_4+x_3x_5}{x_0x_1}\right)^{a_2}\left(\frac{x_1x_4+x_0x_5}{x_2x_3}\right)^{a_2}\left(\frac{x_0x_2+x_1x_3}{x_4x_5}\right)^{c_2},$$

so

$$X_2 = x_2\left(\frac{x_2x_4+x_3x_5}{x_0x_1}\right)^{a_2}\left(\frac{x_1x_4+x_0x_5}{x_2x_3}\right)^{b_2}\left(\frac{x_0x_2+x_1x_3}{x_4x_5}\right)^{c_2},$$

and let

$$X_0 = x_0\left(\frac{x_2x_4+x_3x_5}{x_0x_1}\right)^{a_3}\left(\frac{x_1x_4+x_0x_5}{x_2x_3}\right)^{b_3}\left(\frac{x_0x_2+x_1x_3}{x_4x_5}\right)^{c_3}.$$

Mutating at vertex 0, we compute the exchange relation:

$$X_0X_0' = X_2X_4 + X_3X_5 \implies$$

$$X_0'X_0 = \left(\frac{x_2x_4 + x_3x_5}{x_0x_1}\right)^{a_1+a_2}\left(\frac{x_1x_4 + x_0x_5}{x_2x_3}\right)^{b_1+b_2}\left(\frac{x_0x_2 + x_1x_3}{x_4x_5}\right)^{c_1+c_2}(x_2x_4 + x_3x_5) \implies$$

$$X_0' = x_1\left(\frac{x_2x_4 + x_3x_5}{x_0x_1}\right)^{a_1+a_2-a_3+1}\left(\frac{x_1x_4 + x_0x_5}{x_2x_3}\right)^{b_1+b_2-b_3}\left(\frac{x_0x_2 + x_1x_3}{x_4x_5}\right)^{c_1+c_2-c_3}.$$

So X_0' has $\tau-$presentation with leading term $x_{f_0(n+1)} = x_1$, as desired. This completes the induction. Finally, note that all exponents in the τ-presentation are non-negative by the Laurent phenomenon [FZ]. □

Now that we have exhibited a factorization formula for any cluster variable, we can analyze any sequence of mutations by looking at the corresponding sequence of exponents $\{a, b, c\}$ associated to the cluster variables. In Section 2.2 we give a recursive solution for these exponents for any mutation sequence and then solve for them explicitly in the case of the $123\ldots$ and $1213\ldots$ sequences.

2.2. **Recursion on exponents for τ-mutation sequences.** The construction in the previous section allows for recursive computation of the exponents of cluster variables for any sequence of τ's. By Theorem 2.1, the ordered cluster $C_n(Q)$ has the following form in general:

$$\begin{aligned} C_n(Q) = \{&x_{f_0(n)}A^{a_1}B^{b_1}C^{c_1}, x_{f_1(n)}A^{a_1}B^{b_1}C^{c_1}, x_{f_2(n)}A^{a_2}B^{b_2}C^{c_2},\\ &x_{f_3(n)}A^{a_2}B^{b_2}C^{c_2}, x_{f_4(n)}A^{a_3}B^{b_3}C^{c_3}, x_{f_5(n)}A^{a_3}B^{b_3}C^{c_3}\}. \end{aligned}$$

For the time being, we abuse notation and represent each factor $A^{\cdot}B^{\cdot\cdot}C^{\cdots}$ by an exponent vector $(\cdot, \cdot\cdot, \cdots)$ so $C_n(Q)$ becomes:

$$\begin{aligned} C_n(Q) = \{&x_{f_0(n)}(a_1, b_1, c_1), x_{f_1(n)}(a_1, b_1, c_1), x_{f_2(n)}(a_2, b_2, c_2),\\ &x_{f_3(n)}(a_2, b_2, c_2), x_{f_4(n)}(a_3, b_3, c_3), x_{f_5(n)}(a_3, b_3, c_3)\}. \end{aligned}$$

Using the exchange relation, we can express the action of any $\tau-$mutation in terms of the previous exponents. In particular, we have a recursive method for computing each of the sequences a_j, b_j, c_j. For the dP3 quiver, this yields a much faster algorithm for computing cluster variables than using the exchange relation. The three cases make up the following corollary to the proof of the factorization phenomenon.

Corollary 2.2. (1) *Apply* τ_1.

$$\begin{aligned} C_{n+1}(Q) = \tau_1 \circ C_n(Q) = \{&x_{f_1(n)}(a_2 + a_3 - a_1 + 1, b_2 + b_3 - b_1, c_2 + c_3 - c_1),\\ &x_{f_0(n)}(a_2 + a_3 - a_1 + 1, b_2 + b_3 - b_1, c_2 + c_3 - c_1),\\ &x_{f_2(n)}(a_2, b_2, c_2), x_{f_3(n)}(a_2, b_2, c_2), x_{f_4(n)}(a_3, b_3, c_3),\\ &x_{f_5(n)}(a_3, b_3, c_3)\} \end{aligned}$$

(2) *Apply* τ_2.

$$\begin{aligned} C_{n+1}(Q) = \tau_2 \circ C_n(Q) = \{&x_{f_0(n)}(a_1, b_1, c_1), x_{f_1(n)}(a_1, b_1, c_1), \\ &x_{f_3(n)}(a_1 + a_3 - a_2, b_1 + b_3 - b_2 + 1, c_1 + c_3 - c_2), \\ &x_{f_2(n)}(a_1 + a_3 - a_2, b_1 + b_3 - b_2 + 1, c_1 + c_3 - c_2), \\ &x_{f_4(n)}(a_3, b_3, c_3), x_{f_5(n)}(a_3, b_3, c_3)\} \end{aligned}$$

(3) *Apply* τ_3.

$$\begin{aligned} C_{n+1}(Q) = \tau_3 \circ C_n(Q) = \{&x_{f_0(n)}(a_1, b_1, c_1), x_{f_1(n)}(a_1, b_1, c_1), \\ &x_{f_2(n)}(a_2, b_2, c_2), x_{f_3(n)}(a_2, b_2, c_2), \\ &x_{f_5(n)}(a_1 + a_2 - a_3, b_1 + b_2 - b_3, c_1 + c_2 - c_3 + 1), \\ &x_{f_4(n)}(a_1 + a_2 - a_3, b_1 + b_2 - b_3, c_1 + c_2 - c_3 + 1)\} \end{aligned}$$

This description may be summarized as follows. To compute the next cluster after applying τ_i, flip the leading terms for the cluster variables at vertices position $2i-1$ and $2i-2$ and apply the above recursion to get the exponents.

Next, using the $\tau-$presentation of cluster variables we are able to guess the form of cluster variables appearing in the mutation sequences $123\ldots$ and $1213\ldots$. Verifying these formulas hold is a simple application of the recursion and induction on $C_n(Q)$. Then by the result for the $123\ldots$ sequence and the main result in [Zha12], we have obtained a closed form for the generating function for perfect matchings of Aztec dragons under the weighting scheme of [Spe]. The explicit formula for the $1213\ldots$ sequence will be utilized later in the proof of Theorem 4.1.

Corollary 2.3. *Recall that* $\beta^n = (123)^n$*, and denote the ordered cluster obtained after* n *applications of* β *by* $\beta^n(Q)$*. By ordered, we mean that the* i^{th} *term of* $\beta^n(Q)$ *is the variable at the vertex* i *of* Q*. We have two cases:*

(a) *If* n *is even,*

$$\begin{aligned} \beta^n(Q) = C_{3n}(Q) = \{&x_0 A^{\frac{3n^2}{4}} B^{\frac{3n^2-2n}{4}} C^{\frac{3n^2-4n}{4}}, x_1 A^{\frac{3n^2}{4}} B^{\frac{3n^2-2n}{4}} C^{\frac{3n^2-4n}{4}}, \\ &x_2 A^{\frac{3n^2+2n}{4}} B^{\frac{3n^2}{4}} C^{\frac{3n^2-2n}{4}}, x_3 A^{\frac{3n^2+2n}{4}} B^{\frac{3n^2}{4}} C^{\frac{3n^2-2n}{4}}, \\ &x_4 A^{\frac{3n^2+4n}{4}} B^{\frac{3n^2+2n}{4}} C^{\frac{3n^2}{4}}, x_5 A^{\frac{3n^2+4n}{4}} B^{\frac{3n^2+2n}{4}} C^{\frac{3n^2}{4}}\} \end{aligned} \tag{2.1}$$

(b) *If* n *is odd,*

(2.2)

$$\begin{aligned} \beta_n(Q) = C_{3n}(Q) = \{&x_1 A^{\frac{3n^2+1}{4}} B^{\frac{3n^2-2n-1}{4}} C^{\frac{3n^2-4n+1}{4}}, x_0 A^{\frac{3n^2+1}{4}} B^{\frac{3n^2-2n-1}{4}} C^{\frac{3n^2-4n+1}{4}}, \\ &x_3 A^{\frac{3n^2+2n-1}{4}} B^{\frac{3n^2+1}{4}} C^{\frac{3n^2-2n-1}{4}}, x_2 A^{\frac{3n^2+2n-1}{4}} B^{\frac{3n^2+1}{4}} C^{\frac{3n^2-2n-1}{4}}, \\ &x_5 A^{\frac{3n^2+4n+1}{4}} B^{\frac{3n^2+2n-1}{4}} C^{\frac{3n^2+1}{4}}, x_4 A^{\frac{3n^2+4n+1}{4}} B^{\frac{3n^2+2n-1}{4}} C^{\frac{3n^2+1}{4}}\}. \end{aligned}$$

These expressions allow us to deduce the entire sequence of clusters for the sequence $123123\ldots$.

Corollary 2.4. *Let $\phi^n = (1213)^n$, and denote the ordered cluster obtained after n applications of ϕ by $\phi^n(Q)$. Then:*

$$\phi^n(Q) = C_{4n}(Q) = \{x_0 A^{n(n+1)+1} B^{n+1} C^{n^2}, x_1 A^{n(n+1)+1} B^{n+1} C^{n^2},$$
$$x_2 A^{(n+1)^2} B^{(n+1)^2} C^{n(n+1)}, x_3 A^{(n+1)^2} B^{(n+1)^2} C^{n(n+1)},$$
$$x_4 A^{(n+2)(n+1)} B^{(n+1)(n+2)} C^{(n+1)^2}, x_5 A^{(n+2)(n+1)} B^{(n+1)(n+2)} C^{(n+1)^2}\}$$

Comparing Corollary 2.3 with the main result of [Zha12], we obtain that the generating function (times covering monomial) for $D_{N/2}$ is given by one of the terms in the ordered clusters presented in Equation 2.1 or 2.2.

Corollary 2.5. *Let a_N be the N^{th} term of the $123123\ldots$ sequence. Let $n \in \{1,2,3\}, n \equiv N \pmod 3$. The expression $c(D_{N/2})$ is given by the $(2n-1)^{\text{th}}$ term of the cluster $\beta^{\lceil \frac{N}{3} \rceil}(Q)$.*

3. Existence of explicit formula for τ -mutation sequences

We can compute an explicit formula for the exponents of the cluster produced by a mutation sequence ending in alcove (i, j) of the integer or half-integer cone. By symmetry this is sufficient to obtain a formula for the cluster associated to any alcove. To do so, we first use the results of the previous section to compute the clusters produced by permutations of the original sequence $123\ldots$ studied in [Zha12].

Simple symmetry arguments take care of the case where we apply a permutation $\theta : \{1,2,3\} \to \{1,2,3\}$ to Zhang's original sequence $123\ldots$, as permuting the order of the τ_j's constitutes a relabeling of the quiver. Let $y_n^{123\cdots}$ be the cluster variable produced after n steps ($2n$ total mutations) in the $123\ldots$ sequence. Table 1 gives the corresponding permutation α on the quiver for each permuted sequence such that for any y_n obtained after n steps in the permuted sequence, $y_n = \alpha(y_n^{123\cdots})$. Importantly, the action of α on a subgraph produces a new subgraph of the brane tiling. Therefore, each cluster variable produced in one of the sequences below can be expressed as the weighted matchings of a rotated or reflected Aztec dragon.

Table 1. Permutations of $123\ldots$ and Corresponding α

Sequence	α	Action on the brane tiling
$231231\ldots$	(350241)	60° rotation
$213213\ldots$	$(02)(13)(45)$	reflection over a line of slope $\sqrt{3}$
$132132\ldots$	$(25)(34)$	reflection over a line of slope $\frac{\sqrt{3}}{3}$
$312312\ldots$	$(043)(152)$	120° rotation
$321321\ldots$	$(04)(15)$	reflection over a vertical line

Using this table, we recover the following lemma which is integral to the proof of our main theorem, Theorem 1.1.

Lemma 3.1. *If we can write the cluster variables produced as $y_n = c(G)$ (respectively, $y'_n = c(\sigma G)$) for some subgraph G of the brane tiling for all canonical paths in the integer (I) and half-integer (XII) cones, then we may do the same for any path in regions II-XI by applying the appropriate permutation α to G.*

Proof. Given an alcove $\mathcal{A}$ in region $k \in \{I, \dots, XII\}$, first find the permuted Zhang sequence $(\theta(1)\theta(2)\theta(3)\dots)$ bounding region k. Construct the canonical path P to $\mathcal{A}$ in region k. Then $\theta^{-1}(P)$ lies in either the integer or half-integer cone. To recover the cluster at $\mathcal{A}$, apply the permutation α that corresponds to the permuted Zhang sequence $(\theta(1)\theta(2)\theta(3)\dots)$ in Table 1 to the cluster produced at the end of the canonical path $\theta^{-1}(P)$. Applying α to the graphs that correspond to the cluster at the end of $\theta^{-1}(P)$ proves the lemma. □

Theorem 3.2. *For any alcove (i, j) we can compute an explicit formula for the cluster in terms of i, j.*

At the end of the proof we compute this explicit formula for the cluster variable at vertex 0 corresponding to the alcove (i, j) where $i \equiv j \equiv 0 \pmod 3, i \equiv 0 \pmod 2, i, j \geq 0$.

Proof. If we can find a sequence of mutations ending in alcove (i, j) (in the integer cone I or the half-integer cone XII) which is a concatenation of subsequences of the form in the table, we can then compose the formulae for the cluster variables in Section 2 to obtain the exponents explicitly for these alcoves. Such concatenations are given by the canonical paths first described in Section 1.5 in regions I or XII. Then by the above lemma, this is sufficient to give the explicit formula for any alcove.

Now let us calculate the variable at vertex 0 corresponding to the alcove (i, j) where $i \equiv j \equiv 0 \pmod 3, i \equiv 0 \pmod 2, i, j \geq 0$. The canonical path corresponding to alcove (i, j) is $(123)^{\frac{2j}{3}}(213)^{\frac{i}{3}}$. The cluster variable at vertex 0 after $(213)^{\frac{i}{3}}$ is

$$\alpha(x_2 A^{\frac{3\frac{i}{3}^2+2\frac{i}{3}}{4}} B^{\frac{3\frac{i}{3}^2}{4}} C^{\frac{3\frac{i}{3}^2-2\frac{i}{3}}{4}}) = x_0 A^{\frac{i^2}{12}} B^{\frac{i^2}{12}-\frac{i}{2}} C^{\frac{i^2}{12}-\frac{i}{3}}$$

where α is the permutation $(02)(13)(45)$ obtained from Table 1. We read the cluster after $(123)^{\frac{2j}{3}}$ from Section 2.3. Denote the cluster variables by $\{X_0, X_1, X_2, X_3, X_4, X_5\}$. Then we have:

$$X_0 = x_0 A^{\frac{j^2}{3}} B^{\frac{j^2-j}{3}} C^{\frac{j^2-2j}{3}}$$

$$X_1 = x_1 A^{\frac{j^2}{3}} B^{\frac{j^2-j}{3}} C^{\frac{j^2-2j}{3}}$$

$$X_2 = x_2 A^{\frac{j^2+j}{3}} B^{\frac{j^2}{3}} C^{\frac{j^2-j}{3}}$$

$$X_3 = x_3 A^{\frac{j^2+j}{3}} B^{\frac{j^2}{3}} C^{\frac{j^2-j}{3}}$$

$$X_4 = x_4 A^{\frac{j^2+2j}{3}} B^{\frac{j^2+j}{3}} C^{\frac{j^2}{3}}$$

$$X_5 = x_5 A^{\frac{j^2+2j}{3}} B^{\frac{j^2+j}{3}} C^{\frac{j^2}{3}}$$

Substituting these expressions into the formula for the cluster variable at vertex 0, we obtain the cluster variable at the end of the given canonical path is the following:

$$X_0' = x_0 A^{\frac{j^2}{3}+\frac{i^2}{12}+\frac{j(i)}{3}} B^{\frac{j^2+j}{3}+\frac{i^2}{12}-\frac{i}{2}+\frac{j(i)}{3}} C^{\frac{j^2-j}{3}+\frac{j(i)}{3}+\frac{i^2}{12}-\frac{i}{3}}$$

□

The next corollary illustrates that there are no relations among the τ's other than those stated in Section 1.2. The explicit computation for a specific case is also given in the proof.

Corollary 3.3. $< \tau_1, \tau_2, \tau_3 > \cong \tilde{A}_2$

Proof. Because we can calculate the cluster corresponding to each alcove explicitly, we can set the exponents for each cluster variable equal to 0 and determine when we return to the original cluster. By examination of these explicit formulae it follows that the cluster returns to $\{x_0, x_1, x_2, x_3, x_4, x_5\}$ at alcove (i, j) if and only if $(i, j) = (0, 0)$. Thus the only relations amongst τ_1, τ_2, and τ_3 are those encoded in the lattice, i.e. the relations given by $\tilde{A}_2$. We perform this computation in the case $i \equiv j \equiv 0 \pmod 3, i \equiv 0 \pmod 2, i, j \geq 0$. By the computation in Theorem 3.2, the cluster variable produced entering alcove (i, j) is:

$$X_0' = x_0 A^{\frac{j^2}{3}+\frac{i^2}{12}+\frac{j(i)}{3}} B^{\frac{j^2+j}{3}+\frac{i^2}{12}-\frac{i}{2}+\frac{j(i)}{3}} C^{\frac{j^2-j}{3}+\frac{j(i)}{3}+\frac{i^2}{12}-\frac{i}{3}}.$$

Note that if $X_0' = x_0 \implies \frac{j^2}{3} + \frac{i^2}{12} + \frac{j(i)}{3} = \frac{j^2+j}{3} + \frac{i^2}{12} - \frac{i}{2} + \frac{j(i)}{3} = 0$, subtracting these two equations we get $2j = 3i$, which substituting into the exponent of A gives $\frac{j^2}{3} + \frac{4j^2}{108} + \frac{2j^2}{9} = 0 \implies j = 0 \implies (i, j) = (0, 0)$. So by simply examining the first cluster variable in the cluster when $i \equiv j \pmod 3, i \equiv 0 \pmod 2$ we see that the cluster returns to the initial cluster at alcove (i, j) if and only if $(i, j) = (0, 0)$. Cases for different values of $i, j \pmod 3$ and $i \pmod 2$ follow similarly. □

4. The Integer Cone

Now we return to the original problem of relating cluster variables produced by τ-mutation sequences to subgraphs of the brane tiling, starting with the integer cone of the Coxeter lattice first introduced in Section 1.5. We will first describe a shorthand method for drawing Aztec castles and provide several examples. We will then proceed to prove a recursion on the weights of perfect matchings of these subgraphs utilizing a technique known as graphical condensation first introduced in [Kuo] and further generalized in [Spe]. Finally we will prove a recursion on the covering monomials of the castles, allowing us to complete the proof of the Integer Cone Theorem (Theorem 4.4).

4.1. Hexagonal Notation.

In this section we introduce convenient notation that allows us to define the graphs of interest. Given a six-tuple (a, b, c, d, e, f), we associate the following hexagon illustrated in Figure 8.

In turn, this six-tuple defines a subgraph G of the brane tiling. We use the tuple to define the boundary of the planar graph G in terms of a path in the brane tiling.

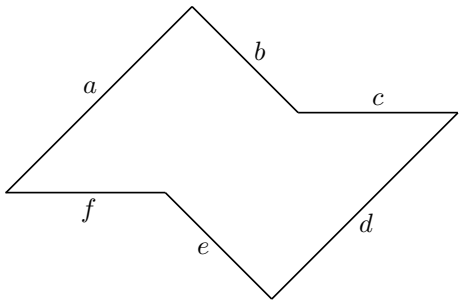

FIGURE 8. The hexagonal notation for a general castle, the sides of which are identified by the tuple (a, b, c, d, e, f).

Begin the boundary path P at some point p, called the basepoint of G, in the brane tiling which is the white vertex in the center of a 6-cycle (see Section 1.1 for terminology). The boundary path consists of six subpaths, each of which will be defined in terms of the cardinal directions naturally associated to the edges of the brane tiling.

For notational convention, if $P = (p_1, p_2, p_3, \ldots)$ and $Q = (q_1, q_2, q_3, \ldots)$ are paths in the brane tiling represented by cardinal directions $p_1, p_2, p_3, \ldots, p_n$ and $q_1, q_2, q_3, \ldots, q_m$, respectively, denote the left-to-right concatenation of the two paths by $PQ = (p_1, p_2, p_3, \ldots, p_n, q_1, \ldots, q_m)$. Likewise, P^i denotes the path P concatenated with itself i times. Furthermore, define the following four-step subpaths illustrated in Figure 9.

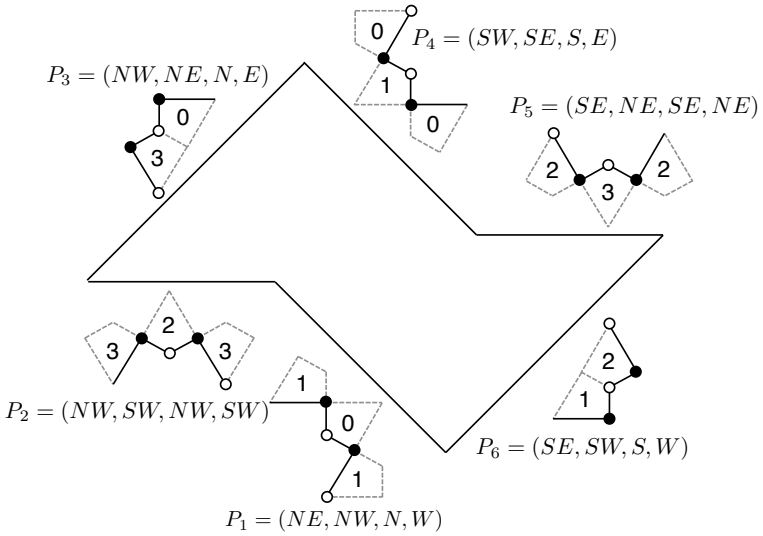

FIGURE 9. The six four-step subpaths that trace out a boundary path P, placed around a castle in hexagonal notation to signify their position in the brane tiling. The subgraph induced by all of the vertices of P is an Aztec castle in the integer cone.

Now, the tuple (a, b, c, d, e, f) corresponds to the following path. Choose p as described above and trace the path

$$P = P_1^e P_2^f P_3^a P_4^b P_5^c P_6^d.$$

Provided that P is a simple closed curve, we define G to be the subgraph induced by all vertices on the boundary path P and in the interior region of P.

The integer order Aztec dragons introduced in [Zha12] fit into this framework with a slight modification. In the hexagonal notation, the n^{th} order Aztec dragon, D_n ($n \in \mathbb{N}$), would have the form exhibited in Figure 10. The x in the left-hand corner signifies that the left-most vertex should be removed from the graph formed by the process defined above. In the six-tuple notation, this removal is denoted by: $\text{x}(n, n-1, 0, n, n-1, 0)$.

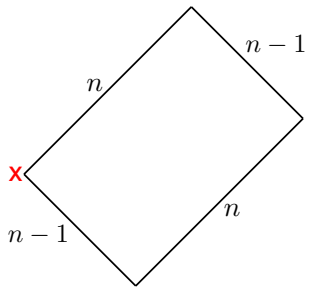

FIGURE 10. An Aztec dragon D_n drawn in hexagonal notation, with a small modification denoted by the red x in the left-hand corner.

Furthermore, observe that if $G = (a, b, c, d, e, f)$, then $\sigma G = (d, e, f, a, b, c)$. In the special case of the Aztec dragon, $\sigma D_n = (n, n-1, 0, n, n-1, 0)\text{x}$, where the x on the right–hand side of the tuple signifies that the rightmost vertex in the graph $(n, n-1, 0, n, n-1, 0)$ should be deleted.

4.2. **Graphs in the Integer Cone.** Utilizing this hexagonal notation, we now define a new family of subgraphs of the brane tiling called **Aztec castles of integer order**. The motivation for this terminology stems from the fact that these castles include the integer order Aztec dragons as a special case. Later we will prove that this family consists of all of the subgraphs of the brane tiling contained in the integer cone.[2]

Definition 3 (Aztec Castle of Integer Order)**.** *Define the (ℓ, k)–Aztec castle of integer order γ_k^ℓ for $\ell \in \mathbb{Z}_{\geq 0}$ and $-3 \leq k \leq \ell - 1$ as follows. Note that addition and scalar multiplication in this case correspond to the standard operations on $\mathbb{Z}^6$.*

$$\gamma_k^\ell = \begin{cases} (2\ell+3, \ell+1, \ell+1, 2\ell+2, \ell, \ell+2) - (k+3)(1,0,1,1,0,1) & \text{if } -3 \leq k < \ell - 1 \\ \sigma D_{\ell+1} = (\ell+1, \ell, 0, \ell+1, \ell, 0)\text{x} & \text{if } k = \ell - 1 \end{cases}$$

[2]A brief discussion on how these graphs were first computed can be found in Problem 6.5 where we utilised a method detailed in [EF].

Note that $\gamma_{-3}^{\ell} = \rho\,\gamma_{-1}^{\ell+1}$, where ρ is the permutation $(03)(12)$, whose action is exhibited in Figure 11.

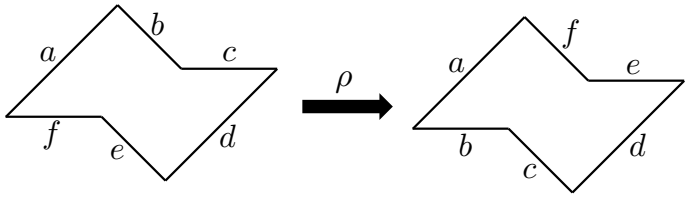

FIGURE 11. The action of the permutation ρ on a subgraph G in hexagonal notation.

Two examples of Aztec castles, $\gamma_0^1 = \sigma\,D_2$ and γ_{-2}^2 are illustrated with their associated hexagonal notation in Figures 12 and 13 respectively.

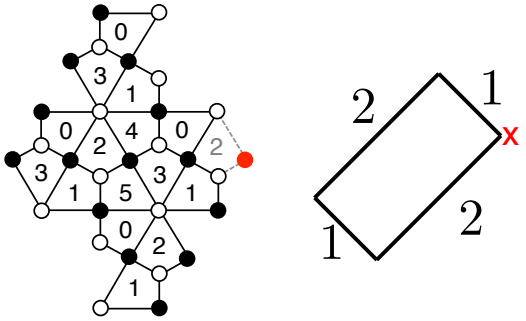

FIGURE 12. The castle $\sigma\gamma_0^1$, also known as the Aztec dragon D_2.

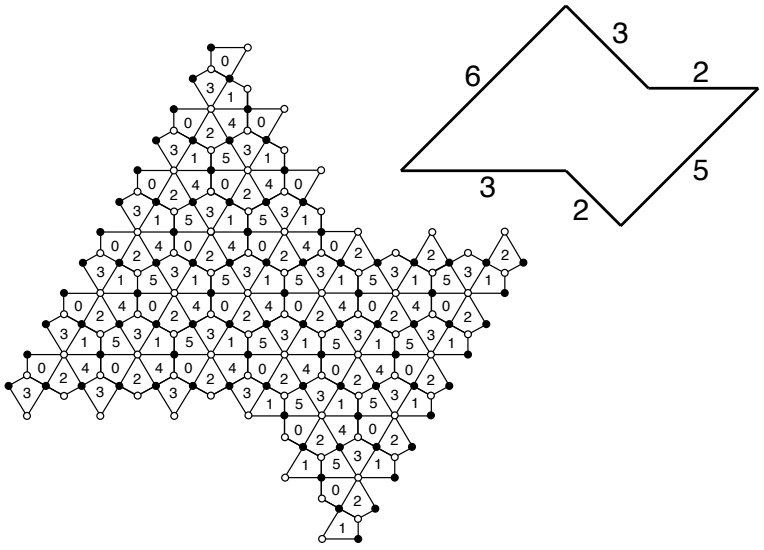

FIGURE 13. The castle γ_{-2}^2 as a subgraph of the dP3 brane tiling with its corresponding hexagonal notation.

4.3. **The Integer Cone Theorem.** Recall the canonical paths and coordinates defined in the integer cone introduced previously in Section 1.5. Denote by $x_{i,j}$ the first cluster variable produced after entering the alcove (i, j) by a canonical path (e.g. if the last step in a canonical path is $\tau_2 = \mu_2 \circ \mu_3$, $x_{i,j}$ is the variable produced by μ_2).

Theorem 4.1. *For all alcoves (i, j) in the integer cone, $x_{i,j}$ is equal to $c(G)$, where G is either an Aztec castle of integer order or a 180° rotation of an Aztec castle of integer order.*

The specific pairing of the alcove (i, j) with the appropriate Aztec castle γ_k^ℓ is proven at the end of this section and is also summarized by the image of the integer cone on the following page in Figure 14. To prove Theorem 4.1, we develop recursions on the weights and covering monomials of Aztec castles.

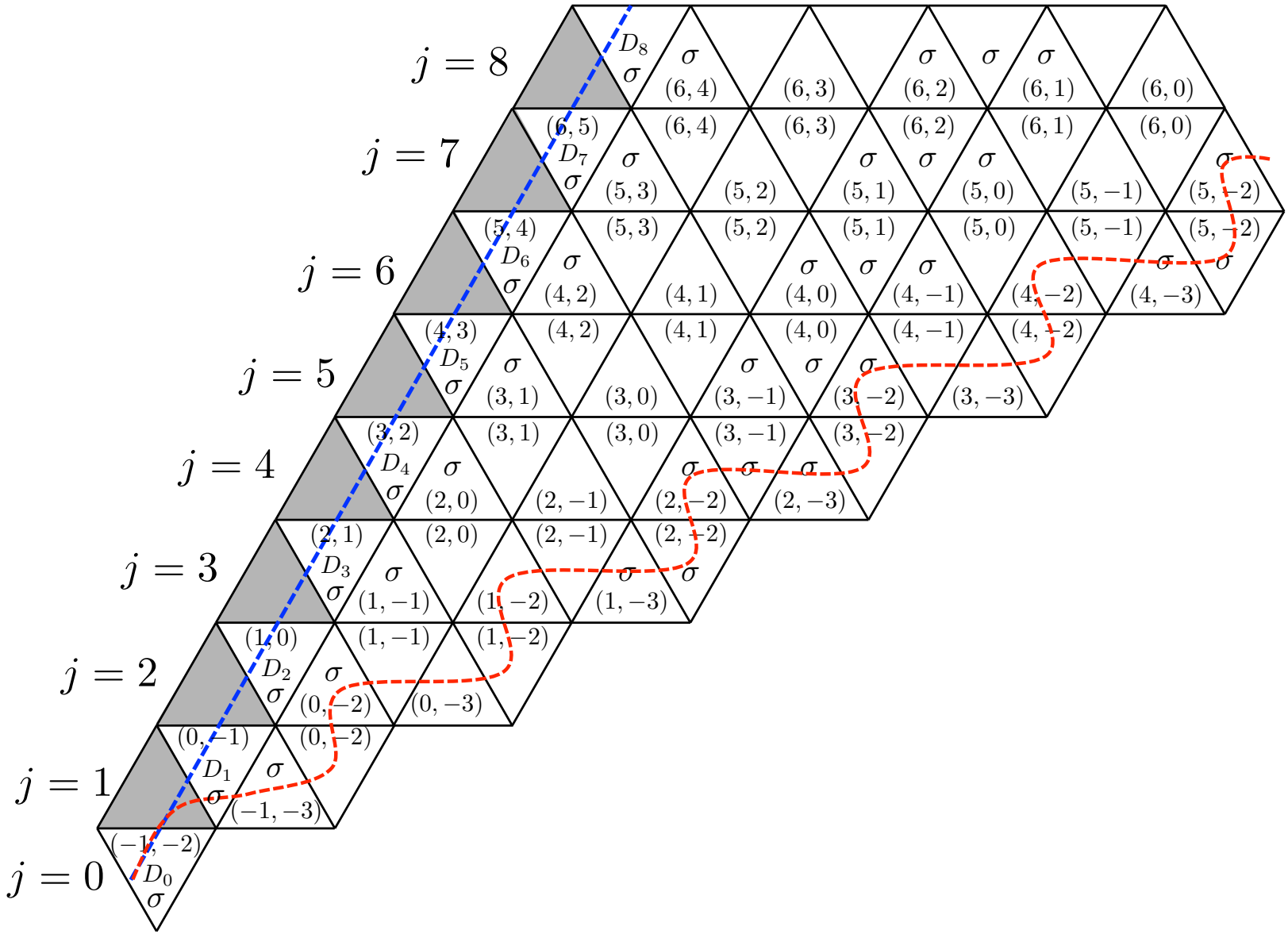

FIGURE 14. The integer cone. Recall that the blue and red paths are $123\ldots$ and $1213\ldots$, respectively. The alcoves are labeled by (ℓ, k) or $\sigma(\ell, k)$, where $x_{i,j} = c(\gamma_k^\ell)$ or $c(\sigma\,\gamma_k^\ell)$, respectively.

4.4. **Condensations on Integer-Order Castles.** The work of detailing recursions on the weights of integer-order castles will rely on a method known as graphical condensation which was first introduced by Kuo in [Kuo] and further generalized by Speyer [Spe]. We will be utilizing Speyer's reformulation of the condensation theorem multiple times throughout this section as well as in Section 5, so it is useful to provide a brief review of the necessary facets.

4.4.1. *The Condensation Theorem.* The condensation theorem relates the weights of a graph G to smaller sections of that same graph by dividing G into nine disjoint sets. This decomposition will form the basis of the recursions on the weights of Aztec castles.

Partition the vertices of a planar bipartite graph G into nine distinct sets:

$$V(G) = C \sqcup N \sqcup S \sqcup W \sqcup E \sqcup NE \sqcup NW \sqcup SE \sqcup SW$$

and assume the following conditions hold:

- The edge connections between the nine sets agree with those illustrated in Figure 15. Thus, there cannot be any edge connecting N, S, E, or W to C and other similar restrictions.
- The boundary vertices must be black in the SW and NE sectors and white in the SE and NW sectors.
- N, S, W, E, and C contain the same number of black and white vertices. In SW and NE, the number of black vertices is one more than the number of white vertices and in SE and NW the number of white vertices is one more than the number of black vertices.

Then:

$$\begin{aligned} w(G)w(C) = {} & w(N \cup NE \cup NW \cup C)w(S \cup SE \cup SW \cup C)w(E)w(W) \\ & + w(E \cup NE \cup SE \cup C)w(W \cup NW \cup SW \cup C)w(N)w(S) \end{aligned}$$

4.4.2. *General Weight Relation.*

Lemma 4.2. *For $\ell \geq 0$ and $-2 \leq k < \ell - 1$, the following relation holds.*

$$w(\gamma_k^\ell)w(\sigma\,\gamma_k^{\ell-1}) = (w(\sigma\,\gamma_{k-1}^{\ell-1})w(\gamma_{k+1}^\ell) + w(\gamma_{k-1}^{\ell-1})w(\sigma\,\gamma_{k+1}^\ell)) \left(\frac{1}{x_0x_1x_2x_3x_4x_5}\right).$$

The proof of Lemma 4.2 requires two general forms of condensations which are now presented in the next two sections.

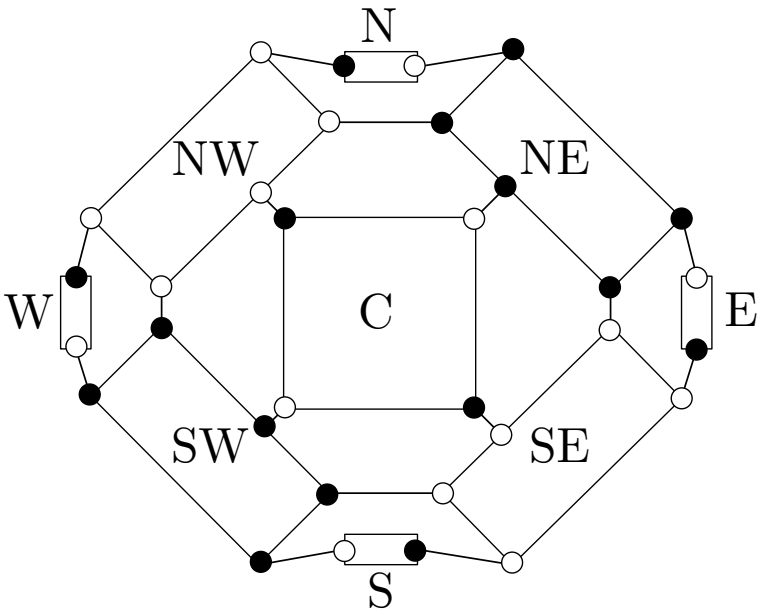

FIGURE 15. The possible allowed edge connections between the nine sets of vertices in a successful application of the condensation theorem. Boundary vertices must be white for the NW and SE sectors and black for the NE and SW sectors.

4.4.3. *First Form of Condensation.* Suppose $G = (a, b, c, d, e, f)$ with all a, b, c, d, e, f positive and basepoint p. We define the components of the decomposition as follows.

- C has basepoint p' at the endpoint of the path P_1 beginning at p and has six-tuple representation $(a-3, b-2, c, d-1, e, f-2)$.
- E and S are empty.
- N consists of the top-most quadrilateral of G, labeled 0, plus the southwest and southeast edges bordering this quadrilateral. Note that $w(N) = \frac{1}{x_1x_2}\frac{1}{x_3x_4}\frac{1}{x_0x_5}$.
- W consists of the left-most quadrilateral in G, which is labeled 3, plus the north and southeast edges bordering this quadrilateral. Note that $w(W) = \frac{1}{x_1x_2}\frac{1}{x_3x_5}\frac{1}{x_0x_4}$.
- Define B_0 to be the first quadrilateral immediately to the right of W which is labeled 3, plus the north edge bordering this quadrilateral. Then SW consists of B_0 and all vertices bounded by G, B_0, and C.
- Define B_1 to be the first quadrilateral southwest of N which is labeled 0, plus the southeast edge bordering the lower black vertex of this quadrilateral. Then NW consists of B_1 and all vertices bounded by G, B_1, C, SW, and W.
- NE consists of all vertices bounded by G, C, N, and NW.
- SE consists of all remaining vertices of G.

These components are also summarized in Figure 16.

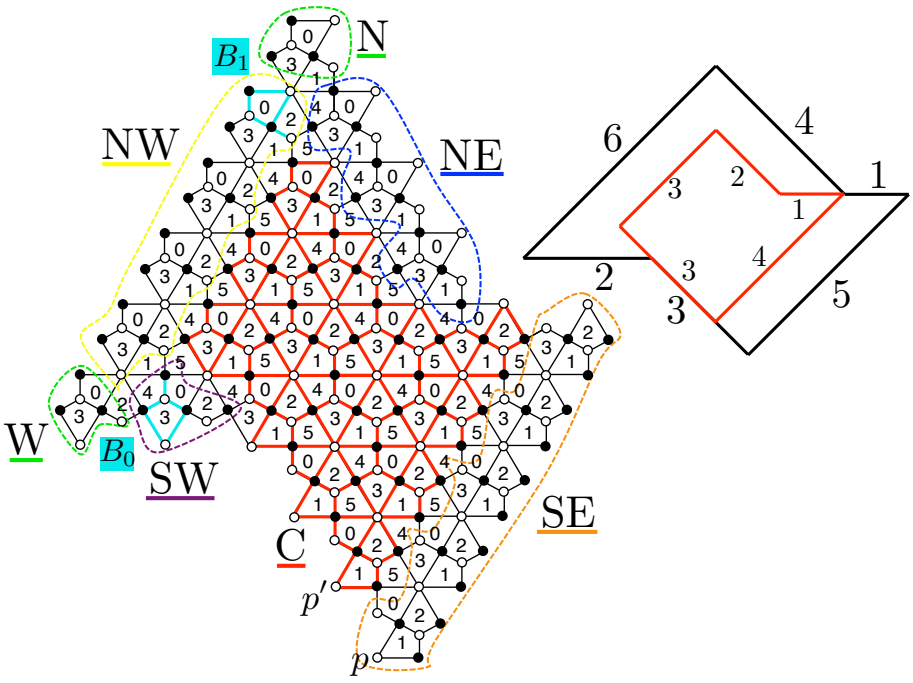

FIGURE 16. Example of the first form of condensation

It is straightforward to verify that all conditions of the condensation theorem are satisfied. For notational convenience, define the quadrants Q_i, $i = 1, \ldots, 4$ of the decomposition as follows. The rightmost equality demonstrates each quadrant in six-tuple notation.

$$Q_1 = S \cup SW \cup SE \cup C = (a-2, b-2, c+1, d, e, f-1)$$
$$Q_2 = W \cup SW \cup NW \cup C = (a-1, b-1, c, d-1, e-1, f)$$
$$Q_3 = N \cup NW \cup NE \cup C = (a-1, b, c-1, d-1, e, f-1)$$
$$Q_4 = E \cup NE \cup SE \cup C = (a-2, b-1, c, d, e+1, f-2)$$

Recalling that $w(W) = w(N) = \frac{1}{x_0x_1x_2x_3x_4x_5}$, we then have the following relation corresponding to this decomposition:

$$w(G)w(C) = \frac{1}{x_0x_1x_2x_3x_4x_5}(w(Q_1)w(Q_3) + w(Q_2)w(Q_4))$$

4.4.4. *Second Form of Condensation.* The second formulation involves G of the form $(\ell+2, \ell+1, 0, \ell+1, \ell, 1)$ with $\ell \in \mathbb{N}$. This decomposition is described explicitly below with an example illustrated in Figure 17.

- C has basepoint p' at the endpoint of the path P_1 beginning at p and has hexagonal representation $\mathrm{x}(\ell, \ell-1, 0, \ell, \ell-1, 0)$. Note that C is the familiar Aztec dragon of integer order D_ℓ.
- S, E, N, and W are identical to the description given earlier in Section 4.4.3

- SW is the vertex originally removed in the construction of $C = D_\ell = \mathrm{x}(\ell, \ell-1, 0, \ell, \ell-1, 0)$.
- Recall the definition of B_1 in 4.4.3. Then NW consists of B_1 and all vertices bounded by G, B_1, C, SW, and W.
- Define B_2 to be the rightmost quadrilateral of G (labeled 2) plus the northwest edge bordering the leftmost black vertex of this quadrilateral. Then SE consists of B_2 and all vertices bounded by G, B_2, and C.
- NE consists of the remaining vertices of G.

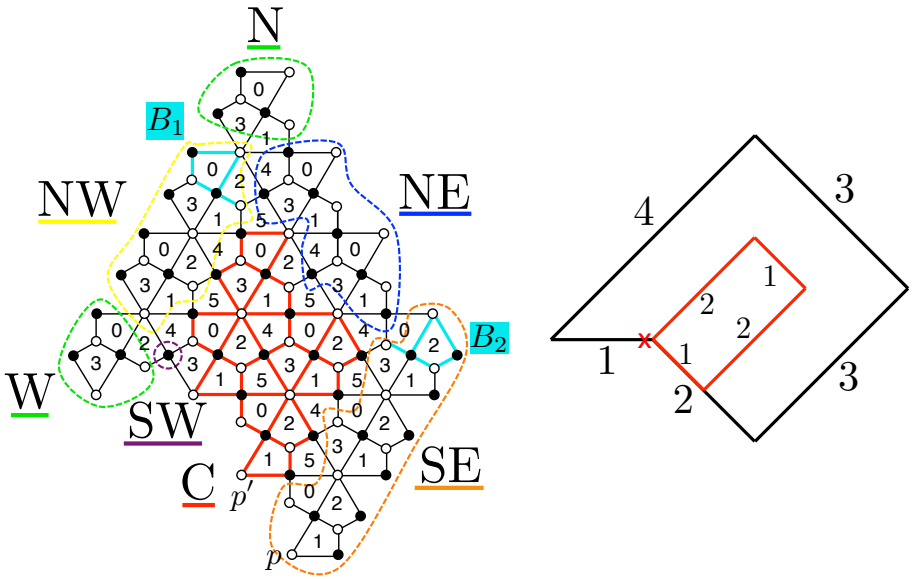

FIGURE 17. Example of the second form of the decomposition.

Again, it is straightforward to verify that the conditions of the condensation theorem are satisfied. Also note that the quadrants have the following form:

$$\begin{aligned} Q_1 &= (\ell, \ell-1, 1, \ell+1, \ell, 0) \\ Q_2 &= (\ell+1, \ell, 0, \ell, \ell-1, 1) = \sigma(Q_1) \\ Q_3 &= \sigma D_{\ell+1} = (\ell+1, \ell, 0, \ell+1, \ell, 0)\mathrm{x} \\ Q_4 &= D_{\ell+1} = \sigma(Q_3) = \mathrm{x}(\ell+1, \ell, 0, \ell+1, \ell, 0) \end{aligned}$$

Using the notation of the previous section, this yields the same relation as before.

$$w(G)w(C) = \frac{1}{x_0x_1x_2x_3x_4x_5}(w(Q_1)w(Q_3) + w(Q_2)w(Q_4))$$

4.4.5. *Proof of the General Weight Relation.* We now give proof of Lemma 4.4.2, the general weight relation among Aztec castles.

Proof. The case $\ell = 0$, $k = -2$ is a base case that is verified separately using a diagram in Section 4.6. Hence for the remainder of the proof, assume $\ell > 0$.

Next, suppose $-2 \leq k < l-2$. Construct the Kuo condensation on $\gamma_k^\ell = (2\ell - k, \ell+1, \ell-k-2, 2\ell-k-1, \ell, \ell-k-1)$ presented in Section 4.4.3. We then make the following observations using the action of σ and the definition of the Aztec castles:

$$\begin{aligned}
C &= (2\ell-k-3, \ell-1, \ell-k-2, 2\ell-k-2, \ell, \ell-k-3) = \sigma\,\gamma_k^{\ell-1} \\
Q_1 &= (2\ell-k-2, \ell-1, \ell-k-1, 2\ell-k-1, \ell, \ell-k-2) = \sigma\,\gamma_{k-1}^{\ell-1} \\
Q_2 &= \sigma Q_1 = \gamma_{k-1}^{\ell-1} \\
Q_3 &= (2\ell-k-1, \ell+1, \ell-k-3, 2\ell-k-2, \ell, \ell-k-2) = \gamma_{k+1}^{\ell} \\
Q_4 &= \sigma\, Q_3 = \sigma\,\gamma_{k+1}^{\ell}
\end{aligned}$$

Plugging in these Q_i into the first condensation verifies this case.

We complete the proof with the case $k = \ell - 2$. By explicit computation, $\gamma_{\ell-2}^\ell = (\ell+2, \ell+1, 0, \ell+1, \ell, 1)$. This graph has the necessary form for the second general Kuo condensation presented in Section 4.4.4. Hence, the center is $D_\ell = \sigma\,\gamma_{\ell-2}^{\ell-1}$. It is routine to verify that $Q_1 = \sigma\,\gamma_{\ell-3}^{\ell-1}$ and $Q_2 = \gamma_{\ell-3}^{\ell-1}$. Finally, by construction, $Q_3 = \sigma\, D_{\ell+1} = \gamma_{\ell-1}^{\ell}$ and $Q_4 = \sigma\,\gamma_{\ell-1}^{\ell}$. Plugging this information in for Q_i into the second condensation equation verifies this case and completes the proof.

□

4.5. **Covering Monomial Relation.** The following lemma will be combined with the weight relation to prove Theorem 4.4.

Lemma 4.3. *For all ℓ, k, where $\ell \geq 0$ and $-2 \leq k \leq \ell - 2$:*

$$\begin{aligned}
m(\gamma_k^\ell)m(\sigma\gamma_k^{\ell-1}) &= (x_0x_1x_2x_3x_4x_5)m(\sigma\gamma_{k-1}^{\ell-1})m(\gamma_{k+1}^\ell) \\
&= (x_0x_1x_2x_3x_4x_5)m(\gamma_{k-1}^{\ell-1})m(\sigma\gamma_{k+1}^\ell)
\end{aligned}$$

Proof. The γ_k^ℓ hexagon has associated side lengths $(2\ell-k, \ell+1, \ell-k-2, 2\ell-1-k, \ell, \ell-1-k)$ when $-2 \leq k \leq \ell-2$ (Section 4.2). We will tackle the $k = \ell-2$ case separately because the graph $\gamma_{\ell-1}^\ell = \sigma D_{\ell+1}$ is a special case. Now, let G be a subgraph of the brane tiling and let $m'(G)$ denote the set of quadrilaterals of the brane tiling included in and bordering G (we represent the quadrilateral marked i by x_i). Then we can rephrase Lemma 4.3 in this new notation as follows. Here the curly brackets $\{\ldots\}$ indicate a multiset.

$$\begin{aligned}
m'(\gamma_k^\ell) \sqcup m'(\sigma\gamma_k^{\ell-1}) &= \{x_0, x_1, x_2, x_3, x_4, x_5\} \sqcup m'(\sigma\gamma_{k-1}^{\ell-1}) \sqcup m'(\gamma_{k+1}^\ell) \\
&= \{x_0, x_1, x_2, x_3, x_4, x_5\} \sqcup m'(\gamma_{k-1}^{\ell-1}) \sqcup m'(\sigma\gamma_{k+1}^\ell)
\end{aligned}$$

Thus if for any i, j we can overlap $m'(\sigma\gamma_{k-1}^{\ell-1})$ and $m'(\gamma_{k+1}^\ell)$ such that

$$[m'(\sigma\gamma_{k-1}^{\ell-1}) \cup m'(\gamma_{k+1}^\ell)] \sqcup \{x_0, x_1, x_2, x_3, x_4, x_5\} = m'(\gamma_k^\ell)$$

and

$$m'(\sigma\gamma_{k-1}^{\ell-1}) \cap m'(\gamma_{k+1}^\ell) = m'(\sigma\gamma_k^{\ell-1}),$$

then the lemma follows.

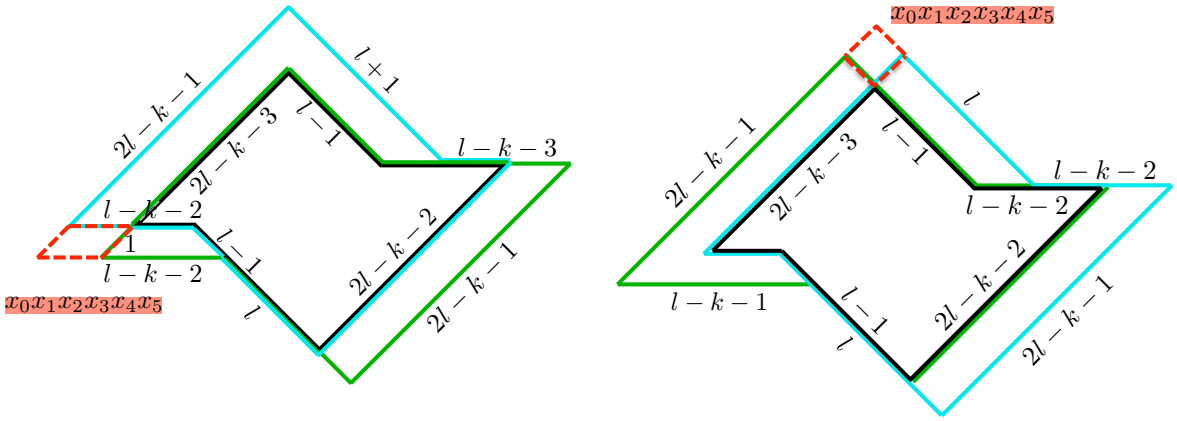

FIGURE 18. The overlapping of the castles γ_{k+1}^{ℓ}[**Blue**] and $\sigma\gamma_{k-1}^{\ell-1}$ [**Green**] on the left with the overlapping of $\sigma\gamma_{k+1}^{\ell}$ and $\gamma_{k-1}^{\ell-1}$ on the right. In both cases, the intersection of the green and blue hexagons is $m'(\sigma\gamma_k^{\ell-1})$ [**Black**], while their union is $m'(\gamma_k^{\ell})$ with one small tip missing which contains the quadrilaterals $\{x_0, x_1, x_2, x_3, x_4, x_5\}$ [**Red**].

Figure 18 illustrates such an overlapping for $k \leq l-3$. The blue hexagon on the left side of the diagram outlines γ_{k+1}^{ℓ}, while the green hexagon is $\sigma\gamma_{k-1}^{\ell-1}$, because the action of σ sends the tuple $(a, b, c, d, e, f) \to (d, e, f, a, b, c)$. Their intersection is $m'(\sigma\gamma_k^{\ell-1})$ and their union is $m'(\gamma_k^{\ell})$, with one **tip** in the brane tiling removed. This tip is outlined in red in the figure, and consists of exactly the quadrilaterals $\{x_0, x_1, x_2, x_3, x_4, x_5\}$ as desired. Collecting these unions and intersections from the left and right hand side of Figure 18 then leads to both equalities in Lemma 4.3

A similar overlapping construction exists for the case $k = \ell - 2$, which is exhibited in Figure 19. For the figure on the left, the larger rectangle with the orange X in its bottom right hand corner is $\gamma_{\ell-1}^{\ell} = D_{\ell+1}$, the hexagon containing the blue quadrilateral is $\gamma_{\ell-3}^{\ell-1}$. We then have

$$[m'(\gamma_{\ell-3}^{\ell-1}) \cup m'(D_{\ell+1})] \sqcup \{x_0, x_1, x_2, x_3, x_4, x_5\} = m'(\gamma_{\ell-2}^{\ell}),$$

and

$$m'(\gamma_{\ell-3}^{\ell-1}) \cap m'(D_{\ell+1}) = m'(D_{\ell}).$$

Hence

$$m(\gamma_{\ell-2}^{\ell})m(\sigma\gamma_{\ell-2}^{\ell-1}) = (x_0x_1x_2x_3x_4x_5)m(\sigma\gamma_{\ell-3}^{\ell-1})m(\gamma_{\ell-1}^{\ell}))$$

as desired. The right-hand side of Figure 19 similarly gives the corresponding relation:

$$m(\gamma_{\ell-2}^{\ell})m(\sigma\gamma_{\ell-2}^{\ell-1}) = (x_0x_1x_2x_3x_4x_5)m(\gamma_{\ell-3}^{\ell-1})m(\sigma\gamma_{\ell-1}^{\ell}).$$

□

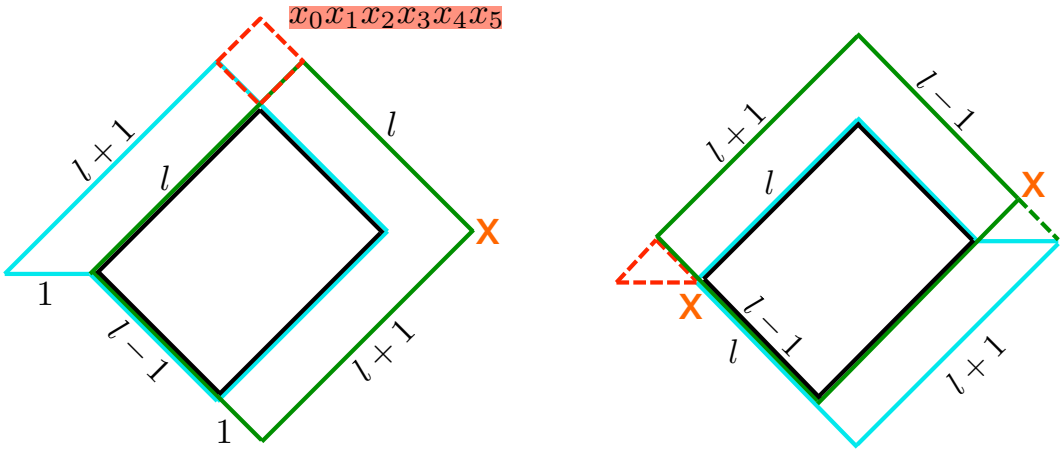

FIGURE 19. The covering monomial overlapping of castles for the case when $k = \ell-2$. The right-side interior blue hexagon (rectangle in this case) is $m'(\sigma\gamma_{\ell-2}^{\ell-1}$ and the intersection of $m'(\gamma_{\ell-3}^{\ell-1})$ and $m'(D_{\ell+1})$. The union of these two plus the quadrilaterals $\{x_0, x_1, x_2, x_3, x_4, x_5\}$ is $m'(\gamma_{l-2}^{\ell})$. Also, in the figure on the right, the triangular region below the dotted green line represents quadrilaterals which are not included by the original figures but are shaded in when considering boundary quadrilaterals, so the argument still holds.

4.6. **Proof of the Integer Cone Theorem.** Now we combine Lemmas 4.2 and 4.3 to prove our main result of this section, Theorem 4.1.

Theorem 4.4 (Main Result 1)**.** *Define the function*

$$f(i) = \begin{cases} 1 & i \equiv 0, 1, 5 \pmod 6 \\ 0 & \textit{else} \end{cases}$$

Define the graph $g(i, j)$ as:

$$g(i,j) = \begin{cases} \sigma^{f(i)}(\gamma_{j-2-\frac{i}{2}}^{j-1}) & i \equiv 0 \pmod 2 \\ \sigma^{f(i)}(\gamma_{j-3-\frac{i+1}{2}}^{j-2}) & i \equiv 1 \pmod 2 \end{cases}$$

Then

$$c(g(i,j)) = x_{i,j}.$$

Proof. Note first that $g(0,1) = \sigma\,\gamma_{-1}^{0} = D_1$, $g(1,1) = \gamma_{-3}^{-1} = \rho\,D_1$, and $g(2,1) = \gamma_{-2}^{0}$. The first two values can be checked explicitly and are also handled in [Zha12]. The value of $g(2,1)$ follows from the decomposition presented in Figure 20. The covering monomial is easily computed by hand.

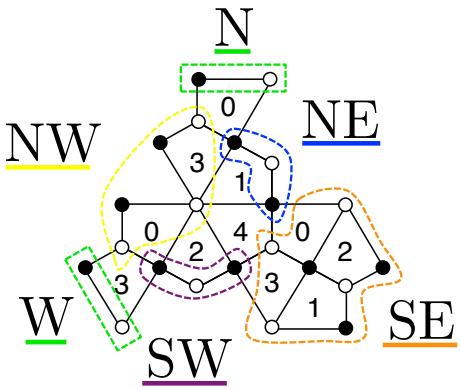

FIGURE 20. The condensation for the base case of γ^0_{-2} which is $g(2,1)$.

Therefore, the theorem holds for the row $j = 1$ in the integer cone. Now let's consider rows higher than $j = 1$. A canonical path falls into one of the three forms described in Section 1.5. By the work in [Zha12], $g(0,j) = D_j = \sigma\,\gamma^{j-1}_{j-2}$.

Now we induct on the rows of the integer cone. Suppose that the theorem holds for row $j-1$. We show that the theorem holds for the row j. This requires handling three cases, one for each type of canonical path. We handle the case $j \equiv 2 \mod 3$ explicitly with the two remaining cases following analogously.

Note that row j of the integer cone consists of $2j+1$ alcoves labeled by coordinates $(0,j)$ to $(2j,j)$. Proving this case has three parts. First we prove the theorem for the following alcoves with odd first coordinate: $(1,j),(3,j),\ldots,(2j-3,j)$. The final odd alcove is a special case that is handled separately. For the remaining alcoves, we will use the exchange relation and the labeling of the quiver at each step to verify that the exchange relation is compatible with the covering monomial and weight relations, which will conclude the proof.

For the first part, note that each of the alcoves $(1,j),(3,j),\ldots,(2j-3,j)$ borders an alcove in the row below it. In general, the alcove (i,j) borders $(i+1,j-1)$. By the inductive hypothesis, the border alcoves $(i+1,j-1)$ have the given table of values.

Alcove $(i+1,j-1)$	$(2,j-1)$	$(4,j-1)$	$(6,j-1)$	$\cdots$
$g(i+1,j-1)$	γ^{j-2}_{j-4}	γ^{j-2}_{j-5}	$\sigma\,\gamma^{j-2}_{j-6}$	$\cdots$

In summary, the p^{th} border alcove has value γ^{j-2}_{j-p-3} or $\sigma\,\gamma^{j-2}_{j-p-3}$. It is the latter iff p is divisible by 3.

Next, by the relations among the τ_j's, recall that any path to the same alcove will yield the same unordered cluster. We can use this to determine that $g(i+1,j-1)$ and $g(i,j)$ are the same up to σ. More specifically, we show that $g(i,j) = \sigma\,g(i+1,j-1)$ if $i \equiv 1 \mod 3$ and is exactly $g(i+1,j-1)$ otherwise. The argument proceeds by induction.

The base case is $i = 1$. We represent the cluster at alcove (i,j) by $\mathcal{C}_{i,j} = \{c_1,c_2,c_3\}$, where c_i denotes the set of cluster variables at vertices v_{2i-1} and v_{2i-2}.

Note that the two members of c_i are related by σ. By this observation, we can abuse notation and replace c_i with one of its elements. With these conventions, we see the following.

$$\mathcal{C}_{1,j} = \{x_{0,j}, x_{0,j-1}, x_{1,j}\};$$
$$\mathcal{C}_{2,j-1} = \{x_{1,j-1}, x_{0,j-1}, x_{2,j-1}\}$$

From the construction of the lattice, $\tau_1 \mathcal{C}_{2,j-1} = \mathcal{C}_{1,j}$. Because the operation τ_1 changes only the first entry of the cluster in the given notation, we can infer that $x_{1,j}$ and $x_{2,j-1}$ are the same up to σ. Next, note that the path to alcove $(2, j-1)$ is given by $\beta^{\frac{2}{3}(j-2)}12|13$ and the path to alcove $(1, j)$ is given by $\beta^{\frac{2}{3}(j-2)+1}1|3$. By the factorization phenomenon, $x_{1,j}$ and $x_{2,j-1}$ have the same exponents. Hence, they differ at most by their leading term, which is determined by the parity of the number of 3's in either path. It is easily checked that this parity is not the same for $x_{1,j}$ and $x_{2,j-1}$, which implies that their leading terms differ by σ. Finally, by the original inductive hypothesis on j, $x_{1,j} = \sigma\, x_{2,j-1} = \sigma\, c(\gamma_{j-4}^{j-2}) = c(\sigma\, \gamma_{j-4}^{j-2}))$ as desired.

The inductive step (on i) follows by a completely analogous argument. With this result, we recover the following table of values.

Alcove (i, j)	$(1, j)$	$(3, j)$	$(5, j)$	$\cdots$
$g(i, j)$	$\sigma\, \gamma_{j-4}^{j-2}$	γ_{j-5}^{j-2}	$\sigma\, \gamma_{j-6}^{j-2}$	$\cdots$

Consequently, $g(2q-1, j) = \gamma_{j-q-3}^{j-2}$ if $q \equiv 2 \mod 3$ and is $\sigma\, \gamma_{j-q-3}^{j-2}$ otherwise, $1 \leq q \leq j-1$. It easily checked that this labeling is consistent with the statement of the theorem.

The second part of the proof handles the alcoves $(2, j), (4, j), (6, j), \ldots, (2j-2, j)$. To prove that the subgraphs corresponding to these alcoves agrees with the theorem, it suffices to show that $g(2r, j) = \sigma\, \gamma_{j-r-2}^{j-1}$ if r is divisible by 3 and is γ_{j-r-2}^{j-1} otherwise. To do so, we demonstrate that the general weight relation from Section 4.4.2 and covering monomial relation from Section 4.5 are compatible with the exchange relation along canonical paths.

We will verify this first directly for the alcoves $(2, j), (4, j)$ and $(6, j)$, which serve as base cases. Before doing so, it will be convenient to introduce notation that represents the seed (the labeling of the quiver and the variables at each vertex) at any stage in the τ-mutation sequence. The seed is represented by the following matrix.

$$\begin{pmatrix} a_0 & a_1 & a_2 \\ X_0 & X_1 & X_2 \\ a_3 & a_4 & a_5 \\ X_3 & X_4 & X_5 \end{pmatrix}$$

Here, $\{a_0, \ldots, a_5\}$ is a permutation of the set $\{0, 1, 2, 3, 4, 5\}$. Starting from the vertex labeled 0 on the initial quiver and reading clockwise, Q currently has the labeling $a_0 - a_1 - a_2 - a_3 - a_4 - a_5$. The entry X_i directly below a_i specifies the

cluster variable at the vertex labeled a_i. For example, $\begin{pmatrix} 0 & 5 & 3 \\ x_0 & x_5 & x_3 \\ 1 & 4 & 2 \\ x_1 & x_4 & x_2 \end{pmatrix}$ specifies the initial cluster. Observe also that because the action of any τ simply swaps antipodal vertices, a_0 and a_3 are either 0 or 1 after any τ-mutation sequence. The analogous statements hold for a_1 and a_4 as well as a_2 and a_5.

The path to the first alcove we consider, $(2, j)$, is given by $\beta^{\frac{2}{3}(j-2)+1}1|32$. By the inductive hypothesis on j, the first part of this proof, and the action of τ_i on the quiver, the seed has the following form immediately before applying the final τ in the given path.

$$\begin{pmatrix} 0 & 5 & 2 \\ c(\sigma\,\gamma_{j-2}^{j-1}) & c(\gamma_{j-4}^{j-2}) & c(\sigma\,\gamma_{j-3}^{j-2}) \\ 1 & 4 & 3 \\ c(\gamma_{j-2}^{j-1}) & c(\sigma\,\gamma_{j-4}^{j-2}) & c(\gamma_{j-3}^{j-2}) \end{pmatrix}$$

The exchange relation for the mutation μ_2, the first mutation in τ_2, is thus:

$$x_{2,j} \cdot c(\sigma\,\gamma_{j-3}^{j-2}) = c(\gamma_{j-2}^{j-1})c(\sigma\,\gamma_{j-4}^{j-2}) + c(\sigma\,\gamma_{j-2}^{j-1})c(\gamma_{j-4}^{j-2})$$

If we set $\ell = j-1$ and $k = j-3$ and multiply the general condensation relation by the covering monomial relation, we recover the previous equation with $x_{2,j}$ replaced by $c(\gamma_{j-3}^{j-1})$. This implies $x_{2,j} = c(\gamma_{j-3}^{j-1})$ as desired.

The same method verifies that $x_{4,j} = c(\gamma_{j-4}^{j-1})$ and $x_{6,j} = \sigma\, c(\gamma_{j-5}^{j-1})$. With this information, we can complete the inductive step.

Suppose that $g(i, j)$ has the desired value up to some alcove (s, j) with $0 \leq s < 2j-2$ and s odd. We verify that the theorem holds for the alcove $(s+1, j)$. Write $s+1 = 2t$ for $t \in \mathbb{N}$. Then based on the value of t modulo 3, we have three cases, one of which we verify explicitly.

Suppose $t \equiv 1 \mod 3$. Then the path to $(2t, j)$ has the form $\beta^{\frac{2}{3}(j-2)+1}1|(321)^{2u}32$, $u \in \mathbb{N}$. Observe that before the application of τ_2, the quiver has the same vertex labeling as before entering the alcove $(2, j)$. Then by the two inductive hypotheses the seed has the following form:

$$\begin{pmatrix} 0 & 5 & 2 \\ c(\sigma\,\gamma_{j-t-1}^{j-1}) & c(\gamma_{j-t-3}^{j-2}) & c(\sigma\,\gamma_{j-t-2}^{j-2}) \\ 1 & 4 & 3 \\ c(\gamma_{j-t-1}^{j-1}) & c(\sigma\,\gamma_{j-t-3}^{j-2}) & c(\gamma_{j-t-2}^{j-2}) \end{pmatrix}$$

Then the exchange relation for μ_2, the first step of τ_2 is given below.

$$\begin{aligned} x_{2t,j} \cdot c(\sigma\,\gamma_{j-t-2}^{j-2}) = {} & c(\sigma\,\gamma_{j-t-3}^{j-2})c(\gamma_{j-t-1}^{j-1}) \\ & + c(\gamma_{j-t-3}^{j-2})c(\sigma\,\gamma_{j-t-1}^{j-1}) \end{aligned}$$

Now set $\ell = j-1$ and $k = j-t-2$ and multiply the general condensation relation by the covering monomial relation. We see that

$$c(\gamma_{j-t-2}^{j-1}) \cdot c(\sigma\,\gamma_{j-t-2}^{j-2}) = c(\sigma\,\gamma_{j-t-3}^{j-2})c(\gamma_{j-t-1}^{j-1}) + c(\gamma_{j-t-3}^{j-2})c(\sigma\,\gamma_{j-t-1}^{j-1})$$

We now solve the equations to see that $x_{2t,j} = c(\gamma_{j-t-2}^{j-1})$, as desired. For $t \equiv 2 \mod 3$, the same process reveals that $x_{2t,j} = c(\gamma_{j-t-2}^{j-1})$. Likewise, if $t \equiv 0 \mod 3$, $x_{2t,j} = c(\sigma\,\gamma_{j-t-2}^{j-1})$, as desired.

We handle separately the alcove with coordinates $(2j-1, j)$, the final alcove with first coordinate odd. The canonical path to this alcove is given by $P = \beta^{\frac{2}{3}(j-2)+1}1|(321)^{\frac{2}{3}(j-2)+1}$. Note that this alcove as well as $(2j-2, j)$ are on the boundary of the integer cone traced by the path $12131213\ldots$. Specifically, $(2j-2, j)$ and $(2j-1, j)$ are intersected by the last two steps of the path $(1213)^{j-1}121$. It follows from Corollary 2.4 that the cluster variables produced by the last two steps of P are related by ρ or $\sigma\rho$. Because the cluster is independent of path, the same must hold true for $x_{2j-2,j}$ and $x_{2j-1,j}$. Using the an argument based on the parity of the number of 2's and 3's in the original path P, we can directly observe that $\rho\, x_{2j-2} = \rho\, c(\gamma_{-1}^{j-1}) = c(\gamma_{-3}^{j-2})$. This is consistent with the construction of g as desired.

Finally, the alcove $(2j, j)$ satisfies $g(2j, j) = \gamma_{-2}^{j-1}$. This is verified with the same argument as used for those alcoves with first coordinate even. This concludes the inductive step for the case $j \equiv 2 \mod 3$. The remaining cases $j \equiv 1, 0 \mod 3$ follow by analogous reasoning. This completes the proof.

□

5. The Half–Integer Cone

Now we study the graphs which appear in the so–called **half–integer cone** first introduced in Section 1.5, which are in perfect duality with the graphs in the integer cone.

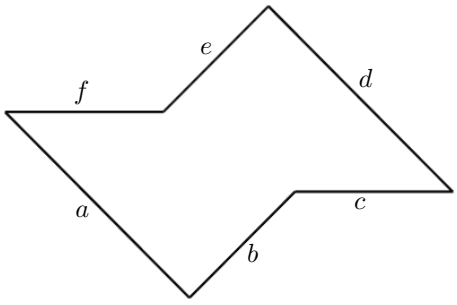

FIGURE 21. The hexagonal notation for a graph in the half-integer cone which is specified by the tuple $[a, b, c, d, e, f]$.

5.1. **Hexagonal Notation.** Given a six-tuple $[a, b, c, d, e, f]$, where we use square brackets to distinguish this from the previous notation, we associate the following hexagon exhibited in Figure 21.

This tuple defines a graph G in the brane tiling. Mark a point p that lies in the center of a 6-cycle (introduced in Section 1.1) in the brane tiling to be the basepoint of G as before. Now define the following four-step subpaths which will make up the boundary of G illustrated in Figure 22.

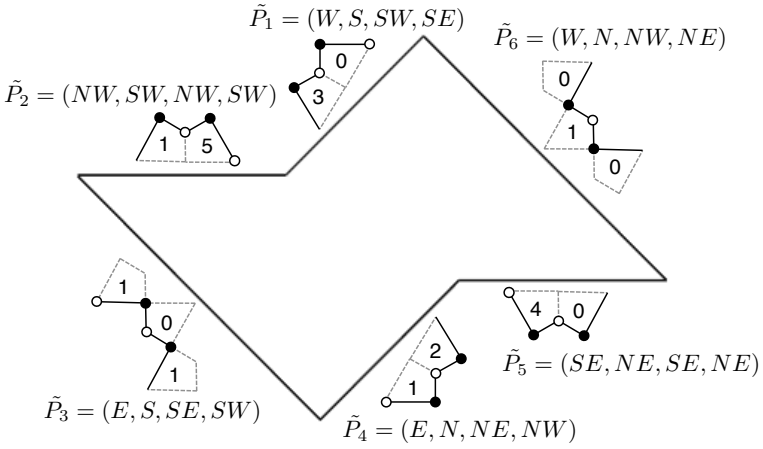

FIGURE 22. The six four-step subpaths that trace out a boundary path $\tilde{P}$ placed around a castle of half-integer order to signify their position in the brane tiling. The subgraph induced by all of the vertices in $\tilde{P}$ is an Aztec castle in the half-integer cone.

Associate the path

$$\tilde{P} = \tilde{P}_1^{e+1} \tilde{P}_2^{f+1} \tilde{P}_3^{a} \tilde{P}_4^{b+1} \tilde{P}_5^{c+1} \tilde{P}_6^{d}$$

which starts at the basepoint p to the tuple $[a, b, c, d, e, f]$. Note that the transition of the path from $\tilde{P}_1$ to $\tilde{P}_2$ as well as $\tilde{P}_4$ to $\tilde{P}_5$ involves tracing out an edge twice. Both of these edges should be deleted from $\tilde{P}$. If $\tilde{P}$ is a simple closed curve after deletion, we define G to be the subgraph induced by all vertices on the boundary path $\tilde{P}$ and in the interior region of $\tilde{P}$.

The half-integer order Aztec dragons fit into this framework with a slight modification. In the hexagonal notation, $\sigma D_{n+\frac{1}{2}}$ would have the following form illustrated in Figure 23. The x in the left-hand corner signifies that the left-most quadrilateral labeled 1 and its sole neighbor labeled 5 in Figure 23 should be removed from the graph formed by the process defined above. In the six-tuple notation, this removal is denoted by $\mathrm{x}[n, n-1, 0, n, n-1, 0]$.

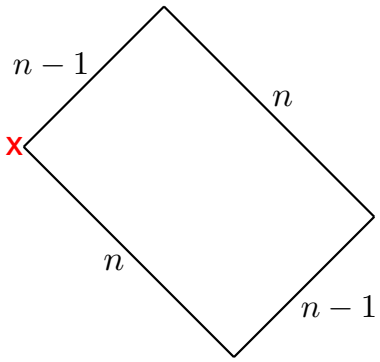

FIGURE 23. The Aztec dragon $D_{n+\frac{1}{2}}$ in hexagonal notation, with a small modification denoted by the red x in the left-hand corner.

Furthermore, observe that if $G = [a, b, c, d, e, f]$, then $\sigma G = [d, e, f, a, b, c]$. In the special case of the Aztec half-dragon, $\sigma D_{n+\frac{1}{2}} = [n, n-1, 0, n, n-1, 0]$x, where the x on the right–hand side of the tuple denotes that the rightmost quadrilateral and its sole neighbor in the graph $[n, n-1, 0, n, n-1, 0]$ should be deleted.

5.2. **Graphs in the Half-Integer Cone.** Here we define the **Aztec castles of half-integer order**, a family of subgraphs of the brane tiling which include the half-integer order Aztec dragons. As before, we will demonstrate that this family is exactly those subgraphs that correspond to mutation sequences in the half-integer cone.

Definition 4 (Aztec Castle of Half-Integer Order)**.** *Define the* (ℓ, k)*–Aztec castle of half-integer order* $\tilde{\gamma}_k^\ell$ *for* $\ell \in \mathbb{Z}_{\geq 0}$ *and* $-3 \leq k \leq \ell - 1$ *as follows. Note that addition and scalar multiplication in this case correspond to the standard operations on* $\mathbb{Z}^6$*.*

$$\tilde{\gamma}_k^\ell = \begin{cases} [2\ell+3, \ell+1, \ell+1, 2\ell+2, \ell, \ell+2] - (k+3)[1,0,1,1,0,1] & \text{if } -2 \leq k < \ell - 1 \\ \sigma D_{\ell+1+\frac{1}{2}} = [\ell+1, \ell, 0, \ell+1, \ell, 0]\text{x} & \text{if } k = \ell - 1 \end{cases}$$

.

Note that $\tilde{\gamma}_{-3}^\ell = \delta\, \tilde{\gamma}_{-1}^{\ell+1}$, where δ is the permutation (25)(34) illustrated in Figure 24.

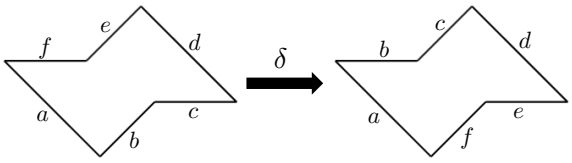

FIGURE 24. The action of δ, the permutation (25)(34), on the half-integer order castles in hexagonal notation.

Two examples of half-integer order Aztec castles, the graphs $\tilde{\gamma}_{-2}^2$ and $\tilde{\gamma}_0^1$, are exhibited in Figures 25 and 26 respectively. Finally, note the duality between γ_k^ℓ

and $\tilde{\gamma}_k^\ell$. When written in six-tuple notation, $\tilde{\gamma}_k^\ell$ is obtained from γ_k^ℓ in a *canonical way* by replacing parentheses with square brackets. In hexagonal representation, this correspondence is illustrated in Figure 27.

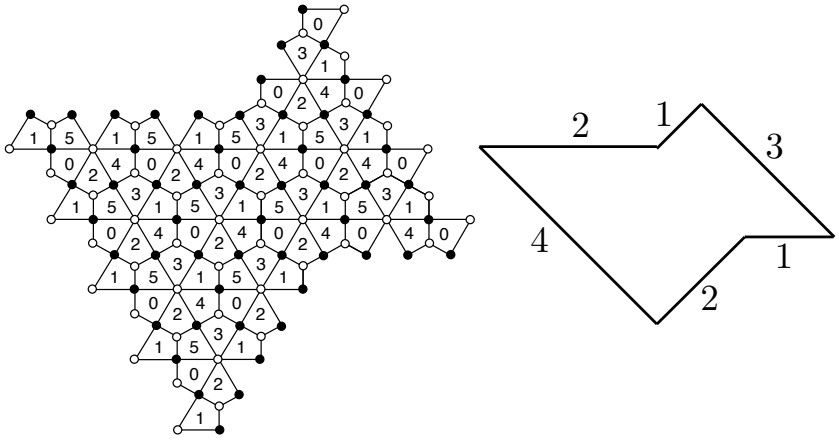

FIGURE 25. The half-integer order castle $\tilde{\gamma}^2_{-2}$ illustrated in the brane tiling and hexagonal notation.

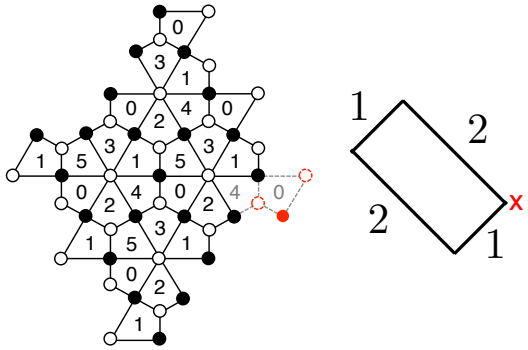

FIGURE 26. The Aztec castle $\tilde{\gamma}^1_0$, which happens to be the Aztec dragon $\sigma\, D_{\frac{5}{2}}$ with corresponding hexagonal notation.

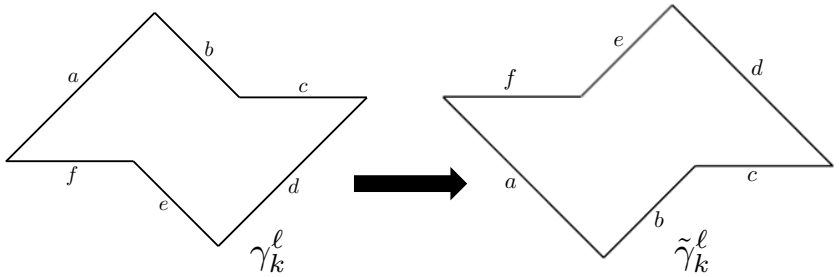

FIGURE 27. The duality between integer order Aztec castles γ_k^ℓ and half-integer order castles $\tilde{\gamma}_k^\ell$.

5.3. **The Half-Integer Cone Theorem.** Recall the coordinates and canonical paths on the half-integer cone first introduced in Section 1.5. As before, define $x_{i,j}$ to be the first variable produced after entering the alcove (i, j) in the half-integer cone by a canonical path. Now we state the main result of this section which is in duality with Theorem 4.1.

Theorem 5.1 (Main Result 2)**.** *For all alcoves (i, j) in the half-integer cone, $x_{i,j}$ is equal to $c(G)$, where G is either an Aztec castle of half-integer order or a* $180°$ *rotation of an Aztec castle of half-integer order.*

The specific pairing of the alcove (i, j) with the appropriate Aztec castle $\tilde{\gamma}_k^\ell$ is stated explicitly at the end of this section. We summarize this pairing with the image on the next page in Figure 28.

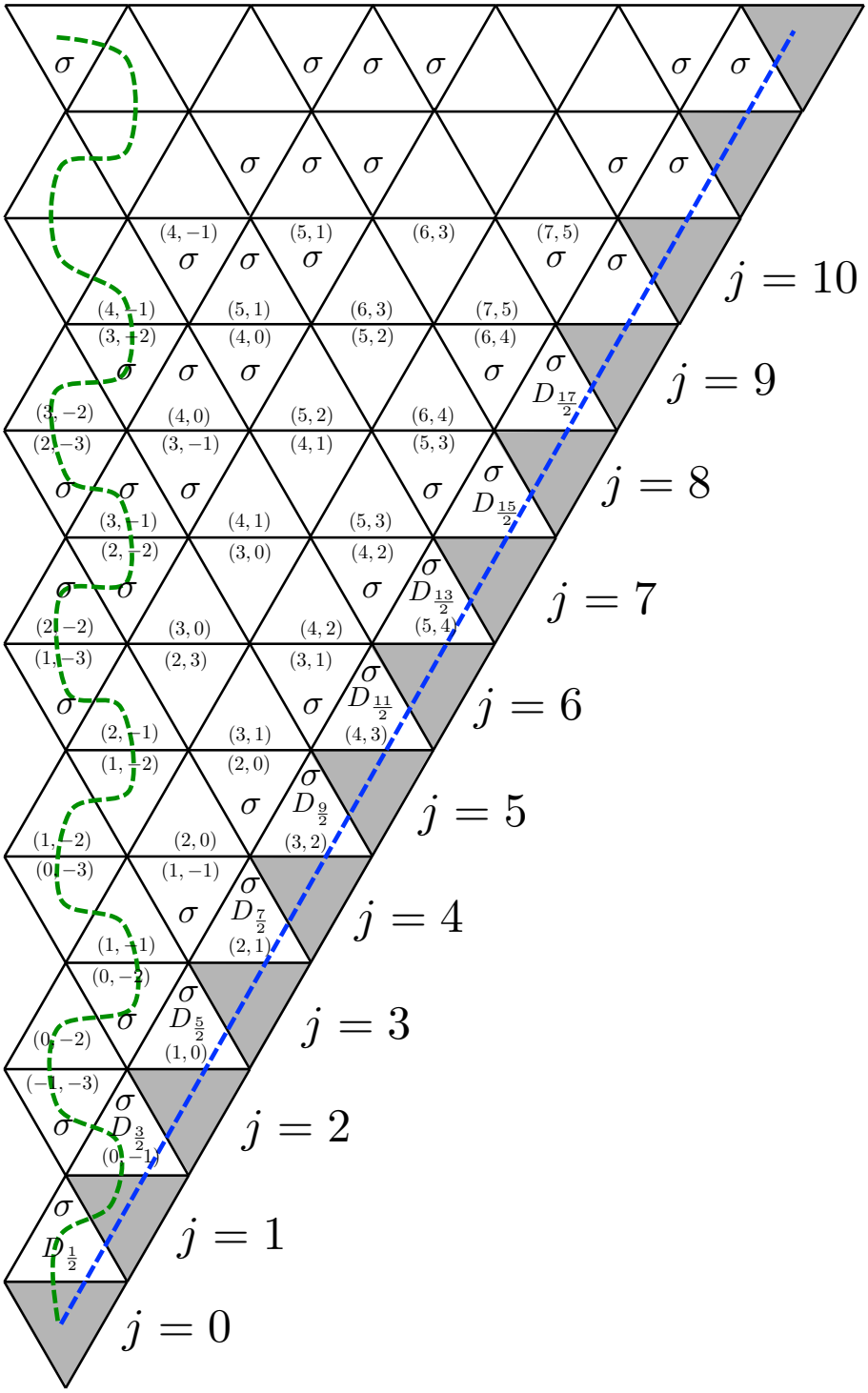

FIGURE 28. The half-integer cone with alcoves labeled by their corresponding half-integer castles, where (ℓ, k) represents $\tilde{\gamma}_k^\ell$ and $\sigma(\ell, k)$ represents $\sigma\,\tilde{\gamma}_k^\ell$. Note that the labeling of the half-integer cone is obtained by flipping the integer cone about the path $123\ldots$ in the Coxeter lattice and converting integer castles to half-integer castles in the canonical way.

5.4. **General Weight Relation.** To prove the main result of this section, we need recursion relations among the weights and covering monomials of half-integer order castles. The weight relation is Lemma 5.2 stated below. Note that this is precisely the statement of Lemma 4.2 with half-integer order castles replacing integer order castles.

Lemma 5.2. *For $\ell \geq 0$ and $-2 \leq k < \ell - 1$, the following relation holds:*

$$w(\tilde{\gamma}_k^\ell) w(\sigma\, \tilde{\gamma}_k^{\ell-1}) = (w(\sigma\, \tilde{\gamma}_{k-1}^{\ell-1}) w(\tilde{\gamma}_{k+1}^\ell) + w(\tilde{\gamma}_{k-1}^{\ell-1}) w(\sigma\, \tilde{\gamma}_{k+1}^\ell)) \left(\frac{1}{x_0 x_1 x_2 x_3 x_4 x_5} \right).$$

To prove this lemma, we must define two general forms of general condensations, similar in manner to the proof of Lemma 4.2. Once these are proven, the proof of Lemma 5.2 mimics the proof of Lemma 4.2.

5.4.1. *First Form of Condensation.* Suppose $G = [a, b, c, d, e, f]$ with all a, b, c, d, e, f positive and basepoint p. Then we define the components of the condensation as follows. It is schematically represented by the hexagonal representation in Figure 29.

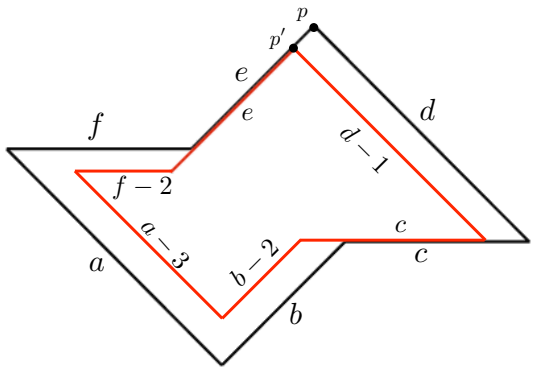

FIGURE 29. The first general condensation illustrated in hexagonal notation, with the center outlined in red.

- Let the basepoint p' of C be the endpoint of the path $\tilde{P}_1$ beginning at p. Then the we let $C = [a-3, b-2, c, d-1, e, f-2]$.
- E and N are empty.
- S consists of the bottom-most quadrilateral, labeled 1, plus the northeast and northwest edges bordering this quadrilateral.
- W consists of the left-most quadrilateral in G, which is labeled 1, plus the south and northeast edges bordering this quadrilateral.
- Define $\tilde{B}_0$ to be the quadrilateral labeled 1 immediately northeast of S plus the northwest edge bordering the higher black vertex of this quadrilateral. Then SE consists of $\tilde{B}_0$ and all vertices bounded by G, C, and $\tilde{B}_0$.
- Define $\tilde{B}_1$ to be the quadrilateral labeled 1 immediately southeast of W plus the northeast edge bordering the rightmost white vertex of this quadrilateral. Then SW consists of $\tilde{B}_1$ and all vertices bounded by G, C, $\tilde{B}_1$, S, and SE.

- NW consists of all vertices in G bounded by C, SW, and W.
- NE consists of all remaining vertices in G.

It is then straightforward to verify that all conditions of the condensation theorem are satisfied. For notational convention, define the quadrants $\tilde{Q}_i$, $i = 1, \ldots, 4$ of the decomposition as follows. Note that this labeling corresponds to applying a flip about a horizontal axis to the first decomposition defined in Section 5.4.1. This is in accordance with the duality which we have observed throughout. It can be verified that the quadrants yield analogous graphs as in the first decomposition. In fact, the transition from Q_i to $\tilde{Q}_i$ is simply replacing parentheses with square brackets. The quadrants are listed below in hexagonal notation. Figure 30 is an example of this condensation.

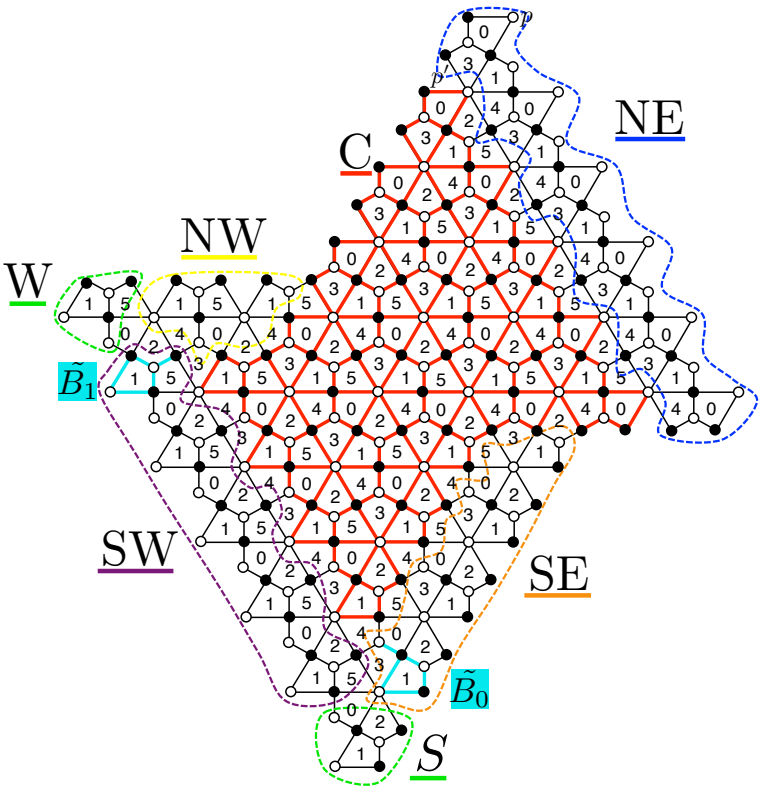

FIGURE 30. Example of the first form of the condensation on castles of half-integer order.

$$\tilde{Q}_1 = N \cup NW \cup NE \cup C = [a-2, b-2, c+1, d, e, f-1]$$
$$\tilde{Q}_2 = W \cup NW \cup SW \cup C = [a-1, b-1, c, d-1, e-1, f]$$
$$\tilde{Q}_3 = S \cup SW \cup SE \cup C = [a-1, b, c-1, d-1, e, f-1]$$
$$\tilde{Q}_4 = E \cup SE \cup NE \cup C = [a-2, b-1, c, d, e+1, f-2]$$

We recover the familiar condensation relation given below.

$$w(G)w(C) = \frac{1}{x_0x_1x_2x_3x_4x_5}(w(\tilde{Q}_1)w(\tilde{Q}_3) + w(\tilde{Q}_2)w(\tilde{Q}_4))$$

5.4.2. *Second Form of Condensation.* The second formulation involves G of the form $[\ell+2, \ell+1, 0, \ell+1, \ell, 1]$ with $\ell \in \mathbb{N}$. This condensation has the hexagonal representation exhibited in Figure 31. We also explicitly define its components. Again, this representation is a flip of the hexagonal representation of the second general decomposition presented in Section 5.4.2.

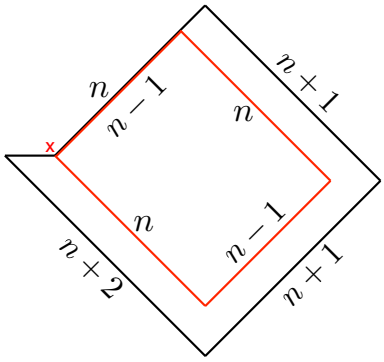

FIGURE 31. The subgraphs covered in the second general condensation are of the form $[\ell+2, \ell+1, 0, \ell+1, \ell, 1]$ with the center defined in red with tuple $\mathrm{x}[\ell, \ell-1, 0, \ell, \ell-1, 0]$.

- The basepoint of C is the endpoint of the path $\tilde{P}_1$ beginning at p. In six-tuple notation, $C = \mathrm{x}[\ell, \ell-1, 0, \ell, \ell-1, 0]$, which is the Aztec dragon $D_{\ell+\frac{1}{2}}$.
- E, W, N, and S are identical to the description given earlier in Section 5.4.1.
- NW consists of the remaining vertices of the quadrilaterals that were deleted from the graph $[\ell, \ell-1, 0, \ell, \ell-1, 0]$ to form $C = D_{\ell+\frac{1}{2}} = \mathrm{x}[\ell, \ell-1, 0, \ell, \ell-1, 0]$.
- Let $\tilde{B}_2$ denote the quadrilateral labeled 1 directly northwest of S plus the northeast edge bordering the rightmost white vertex of this quadrilateral. Then SW consists of $\tilde{B}_2$ and all vertices bounded by G, C, NW, W, and $\tilde{B}_2$.
- Define $\tilde{B}_3$ to be the rightmost quadrilateral of G (labeled 0) plus the southwest edge bordering the leftmost white vertex of this quadrilateral. Then NE consists of $\tilde{B}_3$ and all vertices bounded by G, C, $\tilde{B}_3$.
- SE consists of all remaining vertices of G.

Again, the quadrants are analogous to the quadrants of the second decomposition presented in the previous section.

$$\tilde{Q}_1 = [\ell, \ell-1, 1, \ell+1, \ell, 0]$$
$$\tilde{Q}_2 = [\ell+1, \ell, 0, \ell, \ell-1, 1] = \sigma(\tilde{Q}_1)$$
$$\tilde{Q}_3 = \sigma D_{\ell+1+\frac{1}{2}} = [\ell+1, \ell, 0, \ell+1, \ell, 0]\mathrm{x}$$
$$\tilde{Q}_4 = D_{\ell+1+\frac{1}{2}} = \sigma(\tilde{Q}_3) = \mathrm{x}[\ell+1, \ell, 0, \ell+1, \ell, 0]$$

Finally, we recover the familiar condensation relation below. Figure 32 is an example of this condensation.

$$w(G)w(C) = \frac{1}{x_0x_1x_2x_3x_4x_5}(w(\tilde{Q}_1)w(\tilde{Q}_3) + w(\tilde{Q}_2)w(\tilde{Q}_4))$$

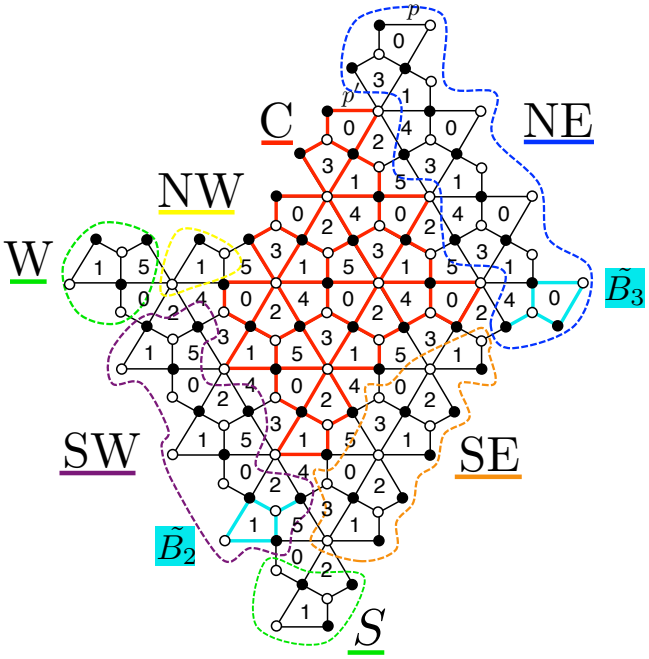

FIGURE 32. Example of the second form of the condensation on castles of half-integer order.

5.5. **Covering Monomial Relation.** Just as with the castles residing within the integer cone, there is an analogous overlapping construction for the covering monomials of half-integer castles. Note that the hexagonal representations of these overlappings are merely flips about a horizontal axis of the overlappings for the integer case.

Lemma 5.3. *For all ℓ, k, where $\ell \geq 0$, and $-2 \leq k \leq \ell - 2$:*

$$m(\tilde{\gamma}\,{}^{\ell}_{k})m(\sigma\tilde{\gamma}\,{}^{\ell-1}_{k}) = (x_0x_1x_2x_3x_4x_5)m(\sigma\tilde{\gamma}\,{}^{\ell-1}_{k-1})m(\tilde{\gamma}\,{}^{\ell}_{k+1})$$
$$= (x_0x_1x_2x_3x_4x_5)m(\tilde{\gamma}\,{}^{\ell-1}_{k-1})m(\sigma\tilde{\gamma}\,{}^{\ell}_{k+1})$$

In a similar manner to the integer castles, Figure 33 exhibits the overlapping construction of covering monomials. The blue hexagon defines $\tilde{\gamma}\,{}^{\ell}_{k+1}$, while the green hexagon outlines $\sigma\tilde{\gamma}\,{}^{\ell-1}_{k-1}$. Using the same notational conventions as in Section 4.5, we see that

$$[m'(\tilde{\gamma}\,{}^{\ell}_{k+1}) \cup m'(\sigma\tilde{\gamma}\,{}^{\ell-1}_{k-1})] \sqcup \{x_0x_1x_2x_3x_4x_5\} = m'(\tilde{\gamma}\,{}^{\ell}_{k}),$$

and

$$m'(\tilde{\gamma}\,{}^{\ell}_{k+1}) \cap m'(\sigma\tilde{\gamma}\,{}^{\ell-1}_{k-1}) = m'(\sigma\tilde{\gamma}\,{}^{\ell-1}_{k}).$$

We can then deduce the first half of the equality in Lemma 5.3 and the second half follows from considering the diagram on the right of Figure 33 which has similar relations.

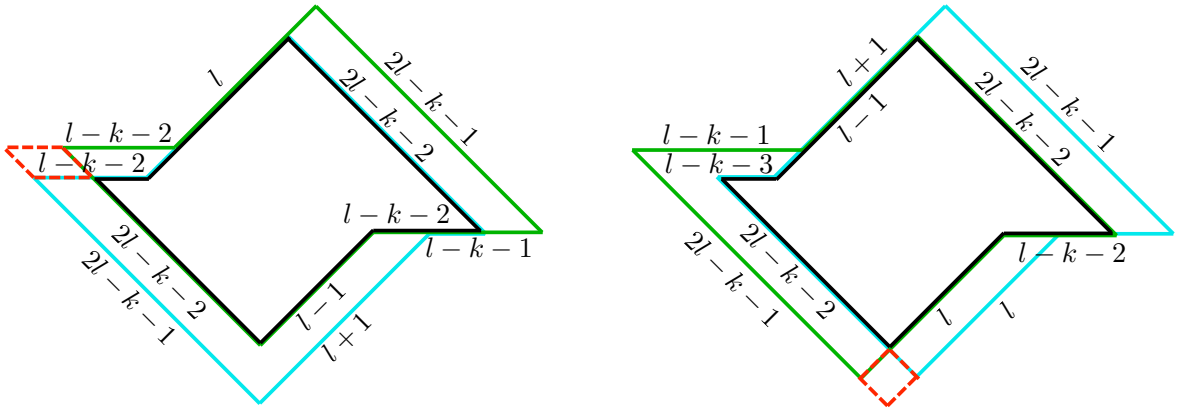

FIGURE 33. The overlapping of the castles $\tilde{\gamma}^{\ell}_{k+1}$[**Blue**] and $\sigma\tilde{\gamma}^{\ell-1}_{k-1}$ [**Green**] on the left with the σ version exhibited on the right. In both cases, the intersection of the green and blue hexagons is $m'(\sigma\tilde{\gamma}^{\ell-1}_{k})$ [**Black**], while their union is $m'(\tilde{\gamma}^{\ell}_{k})$ with one small tip missing which contains the quadrilaterals $\{x_0, x_1, x_2, x_3, x_4, x_5\}$ [**Red**].

Figure 34 illustrates the picture in the case where $k = \ell - 2$, where $\tilde{\gamma}\,{}^{\ell}_{\ell-1}$ is a half-integer order Aztec dragon, and the X signifies two quadrilaterals removed, where analogous relations (Figure 19) to the integer cone case hold.

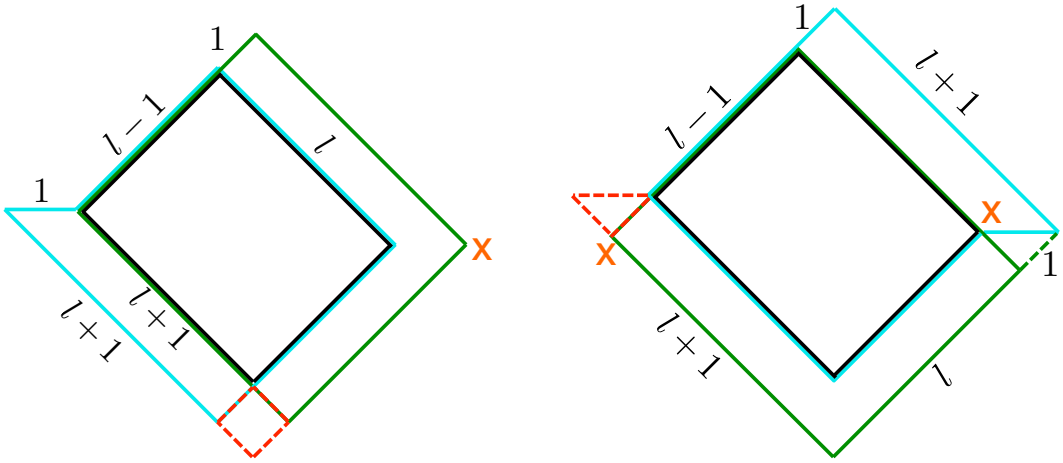

FIGURE 34. The covering monomial overlapping of half integer order castles in the case where $k = \ell - 2$. The dotted green line has the same purpose as described in the caption to Figure 19.

5.6. **Proof of the Half-Integer Cone Theorem and Main Theorem.** Theorem 5.4 is a more precise formulation of the main result of this section.

Theorem 5.4 (Main Result 2)**.** *Let*

$$f(i) = \begin{cases} 1 & \text{iff } i \equiv 0, 1, 5, 6 \\ 0 & \text{else} \end{cases}$$

Define the graph $\tilde{g}(i,j)$ *as:*

$$\tilde{g}(i,j) = \begin{cases} \sigma^{f(i)}(\tilde{\gamma}^{j-1}_{j-2-\frac{i}{2}}) & i \equiv 0 \pmod 2 \\ \sigma^{f(i)}(\tilde{\gamma}^{j-2}_{j-3-\frac{i+1}{2}}) & i \equiv 1 \pmod 2 \end{cases}$$

Then

$$c(\tilde{g}(i,j)) = x_{i,j}.$$

This theorem follows using Lemmas 5.2 and 5.3 along with applying the same techniques as in Section 4.6 [3].

With the above result, Lemma 3.1, implies that our main theorem, Theorem 1.1, is proven by applying the appropriate permutation α for alcoves in regions II - XI of the Coxeter lattice. Such α are given in Table 1.

[3]Gregg Musiker suggests analyzing the duality discussed in this section further. There might be an algebraic duality alongside the graph theoretic duality between integer and half-integer order Aztec castles that could lead to an alternate (and perhaps simpler) proof of Theorem 5.1.

6. Further Questions

Associating subgraphs to the cluster variables produced by τ-mutation sequences on the dP3 quiver presents a foundation from which to explore several promising directions. We now summarize some possibilities for future investigation.

Problem 6.1. *To any matching of a planar bipartite graph G it is possible to associate a corresponding height function on the set of matchings of G, see for example* [Ken03]*, or* [CY10]*. In* [JMZ]*, it is proven that if we enrich our quiver with principal coefficients, the cluster variables produced by the sequence $123\cdots$ are still given by the weighted matchings of Aztec dragons where the coefficients correspond to the height of each perfect matching. In particular, Gregg Musiker conjectures that Aztec castles equipped with height functions also account for principal coefficients.*

Problem 6.2. *In* [CY10] *a domino-shuffle is outlined on the dP3 brane tiling; what happens when this shuffle is applied to perfect matchings of Aztec castles? Is there a simple way to see that the number of these matchings is a power of 2? Even if the shuffling does not give us perfect matchings of other Aztec castles, it could give a new class of subgraphs of the brane tiling whose number of perfect matchings are a power of 2.*

Problem 6.3. *Now that we have analyzed τ-mutation sequences, it is natural to try to extend the work to further mutation sequences on the dP3 quiver, and in particular to toric sequences (mutating only at vertices with 2 incoming and 2 outgoing arrows) that are not τ-mutation sequences. While the factorization phenomenon no longer occurs in these cases, a search for subgraphs with appropriate weighted enumerations of perfect matchings is still of interest.*

Problem 6.4. *Al Garver suggests looking at certain products of cluster variables produced by $\tau-$mutation sequences, as they encode data on pairs of perfect matchings of Aztec castles. Specifically, given two such cluster variables x_{ij} and x_{kl}, if we may write $x_{ij}x_{kl} = \sum_e c_e x_e$, where the x_e's are cluster variables, how do the coefficients c_e encode combinatorial data on superpositions of perfect matchings of the castles associated to x_{ij} and x_{kl}?*

Problem 6.5. *This research project was jumpstarted by applying the method for constructing shadows as outlined in Sections 4 and 7.3 of* [EF] *by Richard Eager and Sebastián Franco. Their work presents two algorithms for computing subgraphs corresponding to toric mutations. During this investigation, a discrepency between the graphs obtained by these two methods was observed, for instance in the special case of the τ-sequence $1213\ldots$, but this was soon resolved through a private discussion with Musiker and Franco* [FM]*. In spite of this issue, the method was still instrumental in allowing us to construct the Aztec castles appearing in this paper. This and other observations suggest that there is much work to be done in providing a mathematical basis to the algorithm – one which could not only shed light on the connections between the combinatorics of cluster algebras and gauge/string theory*

duality, but also immediately lead to combinatorial interpretations of the type given in this paper for a wide variety of quivers and their associated brane tilings.

Acknowledgments

This research was conducted during the 2013 REU in Combinatorics at the University of Minnesota, Twin Cities. The authors would first like to thank Gregg Musiker for suggesting and supervising this project, having several invaluable discussions about the research, demonstrating to us the Eager–Franco method, and commenting on drafts. We would also like to thank Gregg Musiker, Pavlo Pylyavskyy, Joel Lewis, and Dennis Stanton for mentoring the REU. We are grateful that Pavlo Pylyavskyy pointed out the connection to the Coxeter lattice used throughout the paper and that Joel Lewis provided some insightful observations on the factorization phenomenon. The authors would like to thank Thomas McConville for a useful conversation regarding canonical paths, and Sebastián Franco for correspondence regarding the methods in his work with Richard Eager. Finally thanks goes to our graduate student mentor Alexander Garver for numerous fruitful conversations and for commenting diligently on drafts of the manuscript. The research was supported by NSF grants DMS-1067183 and DMS-1148634.

References

[CY10] C. Cottrell and B. Young. Domino shuffling for the Del Pezzo 3 lattice. *ArXiv e-prints*, October 2010. `arXiv:1011.0045`.

[EF] R. Eager and S. Franco. Colored BPS Pyramid Partition Functions, Quivers and Cluster Transformations. *JHEP*, 1209:038.

[FG] V. V. Fock and A. B. Goncharov. Moduli spaces of local systems and higher Teichmuller theory. *Publications Mathematiques de lInstitut des Hautes Etudes Scientifiques*, 103:211.

[FHK$^+$] S. Franco, A. Hanany, K. D. Kennaway, D. Vegh, and B. Wecht. Brane dimers and quiver gauge theories. *JHEP*, 0601:096.

[FM] S. Franco and G. Musiker. private communication.

[FZ] S. Fomin and A. Zelevinsky. Cluster algebras I: Foundations. *Journal of the American Mathematical Society*, 15(2):497–529.

[GK12] A. Goncharov and R. Kenyon. Dimers and Cluster Integrable Systems. *ArXiv Mathematics e-prints*, November 2012. `arXiv:math/1107.5588`.

[HS] A. Hanany and R. Seong. Brane Tilings and Reflexive Polygons. *Fortsch.Phys.*, 60:695–803.

[Jeo11] I. Jeong. Bipartite Graphs, Quivers, and Cluster Variables . 2011. URL: `http://www.math.umn.edu/~reiner/REU/Jeong2011.pdf`.

[JMZ] I. Jeong, G. Musiker, and S. Zhang. Brane Tilings and Cluster Algebras I. *In preparation.*

[JMZ13] I. Jeong, G. Musiker, and S. Zhang. Gale-Robinson Sequences and Brane Tilings. *DMTCS proc. AS*, pages 737–748, 2013. URL: `http://www.liafa.jussieu.fr/fpsac13/pdfAbstracts/dmAS0169.pdf`.

[Kel08] B. Keller. Cluster algebras, quiver representations and triangulated categories. *ArXiv e-prints*, July 2008. `arXiv:0807.1960`.

[Ken03] R. Kenyon. An introduction to the dimer model. *ArXiv Mathematics e-prints*, October 2003. `arXiv:math/0310326`.

[Kuo] E. H. Kuo. Applications of Graphical Condensation for Enumerating Matchings and Tilings. *Theoretical Computer Science*, 319:29–57.

[LS] K. Lee and R. Schiffler. A Combinatorial Formula for Rank 2 Cluster Variables. *Journal of Algebraic Combinatorics*, 37:67–85.

[MS] G. Musiker and R. Schiffler. Cluster expansion formulas and perfect matchings. *Journal of Algebraic Combinatorics*, 32:187–209.

[Mus] G. Musiker. A graph theoretic expansion formula for cluster algebras of classical type. *Annals of Combinatorics*, 15:147–184.

[Rou] R. Rouquier. Weyl groups, affine Weyl groups, and reflection groups. URL: `http://www.math.ucla.edu/~rouquier/papers/weyl.pdf`.

[Spe] D. E Speyer. Perfect Matchings and the Octahedron Recurrence. *Journal of Algebraic Combinatorics*, 25:309–348.

[SW] D. Speyer and L. K. Williams. The tropical totally positive Grassmannian. *Journal of Algebraic Combinatorics*, 22:189–210.

[Zel07] A. Zelevinsky. What is ... a Cluster Algebra? *Notices of the AMS*, 54:1494–1495, 2007.

[Zha12] S. Zhang. Cluster Variables and Perfect Matchings of Subgraphs of the dP_3 Lattice . 2012. URL: `http://www.math.umn.edu/~reiner/REU/Zhang2012.pdf`.

Department of Mathematical Sciences, Durham University, Durham DH1 3LE, UK

E-mail address: `megan.leoni@gmail.com`

Department of Mathematics, Harvard University, Cambridge, MA

E-mail address: `sethneel@college.harvard.edu`

Department of Mathematics, Louisiana State University, Baton Rouge, Louisiana 70803

E-mail address: `pturne7@tigers.lsu.edu`